TECHNICAL REPORT 91-31

GRIMSEL TEST SITE

A SIMPLE TRANSPORT MODEL FOR THE GRIMSEL MIGRATION EXPERIMENTS

F. HERZOG

SEPTEMBER 1991

PSI, Würenlingen and Villigen

nagra National Cooperative for the Disposal of Radioactive Waste

TECHNICAL REPORT 91-31

GRIMSEL TEST SITE

A SIMPLE TRANSPORT MODEL FOR THE GRIMSEL MIGRATION EXPERIMENTS

F. HERZOG

PSI, Würenlingen and Villigen

SEPTEMBER 1991

GRIMSEL TEST SITE/SWITZERLAND
A JOINT RESEARCH PROGRAM BY

- NAGRA - National Cooperative for the Storage of Radioactive Waste, Wettingen, Switzerland
- BGR - Federal Institute for Geoscience and Natural Resources, Hannover, Federal Republic of Germany
- GSF - Research Centre for Environmental Sciences, Munich, Federal Republic of Germany

Hardstrasse 73, CH-5430 Wettingen/Switzerland, Telephone + 41-56-37 11 11

FOREWORD

Concepts for the disposal of radioactive waste in geological formations lay great weight on acquiring extensive knowledge of the proposed host rock and the surrounding rock strata. For this reason, Nagra has, since May 1984, been operating the **Grimsel Test Site (GTS)** which is located at a depth of 450 m in the crystalline rock of the Aare Massif of the Central Swiss Alps. The general objectives of the research being carried out in this underground laboratory include

- the build-up of know-how in planning, performing and interpreting field experiments in various scientific and technical disciplines and

- the acquisition of practical experience in the development of investigation methodologies, measuring techniques and test equipment which will be of use during actual repository site explorations.

The GTS is operated by Nagra and, on the basis of a German-Swiss co-operative agreement, various experiments are carried out by Nagra, the "Bundesanstalt für Geowissenschaften und Rohstoffe, Hannover" (BGR) and the "Forschungszentrum für Umwelt und Gesundheit, München" (GSF). The Grimsel projects of both GSF and BGR are supported by the German Federal Ministry for Research and Technology (BMFT). NTB 85-46 (German version NTB 85-47) provide an overview of the German-Swiss investigation programme. In a special issue of the Nagra Bulletin 1988 (German version "Nagra Informiert 1+2/1988") the status of the programme up to 1988 is described.

The **Radionuclide Migration Experiment (MI)** is the most significant contribution from Nagra to the Grimsel programme. MI is a multidisciplinary study aimed at investigating solute transport in fractured media. Extensive field work is complemented by a substantial programme of hydrodynamic, chemical and transport modelling, along with supporting laboratory studies. This project, initiated in 1985 and currently planned to be terminated in 1994, was initially conceived as a collaborative project between Nagra and the Paul Scherrer Institute (PSI). Since 1987, radiotracer field tests have also been carried out with the Institute of Hydrology of GSF Munich-Neuherberg. In 1989 a bilateral collaboration agreement was signed with the Japanese Power Reactor and Nuclear Fuel Development Corporation (PNC) and the support under this cooperation resulted in a substantial extension of the Grimsel Radionuclide Migration project.

VORWORT

Bei Konzepten, welche die Endlagerung radioaktiver Abfälle in geologischen Formationen vorsehen, ist die Kenntnis des Wirtgesteins und der angrenzenden Gesteinsschichten von grundlegender Bedeutung. Die Nagra betreibt deshalb seit Mai 1984 das **Felslabor Grimsel (FLG)** in 450 m Tiefe im Kristallin des Aarmassivs. Die generelle Zielsetzung für die Arbeiten in diesem System von Versuchsstollen umfasst insbesondere

- den Aufbau von Know-how in der Planung, Ausführung und Interpretation von Untergrundversuchen in verschiedenen wissenschaftlichen und technischen Fachgebieten, und

- den Erwerb praktischer Erfahrung in der Entwicklung und der Anwendung von Untersuchungsmethoden, Messverfahren und Messgeräten, die für die Erkundung von potentiellen Endlagerstandorten in Frage kommen.

Im Felslabor der Nagra werden, auf der Basis eines deutsch-schweizerischen Zusammenarbeitsvertrages, verschiedene Versuche von den beiden deutschen Partnern Bundesanstalt für Geowissenschaften und Rohstoffe, Hannover (BGR) und Forschungszentrum für Umwelt und Gesundheit GmbH, München (GSF) durchgeführt. Das Deutsche Bundesministerium für Forschung und Technologie (BMFT) fördert die Arbeiten der BGR und der GSF im FLG. Der NTB 85-47 (englische Version NTB 85-46) enhält eine Uebersicht des FLG und die Zusammenfassung der Untersuchungsprogramme mit Status August 1985. In der Ausgabe 1+2/1988 des Heftes "Nagra informiert" bzw. der englischen Spezialausgabe "Nagra Bulletin 1988" ist der Stand der FLG Arbeiten anfangs 1988 beschrieben.

Der **Migrationsversuch (MI)** ist ein sehr wesentlicher Beitrag zum Grimsel Programm. MI ist ein multidisziplinäres Experiment zur Untersuchung des Transportverhaltens von Radionukliden in geklüftetem Fels. Die ausgedehnten Feldversuche werden unterstützt durch ein umfangreiches Programm zur hydrodynamischen und chemischen Charakterisierung des MI-Bereichs und zur Modellierung der Transportprozesse sowie durch ergänzende Laboruntersuchungen. Das 1985 begonnene und, gemäss jetziger Planung, bis 1994 dauernde Projekt MI war ursprünglich als gemeinsames Vorhaben der Nagra und des Paul Scherrer Instituts (PSI) konzipiert worden. Seit 1987 führt das Institut für Hydrologie der GSF, München-Neuherberg die Radiotracer-Analysen bei den Feldversuchen durch. Im Jahre 1989 unterzeichnete dann Nagra mit der japanischen Power Reactor and Nuclear Fuel Corporation (PNC) einen Vertrag zur Beteiligung der PNC am Migrationsversuch, wodurch eine wesentliche Erweiterung des Untersuchungsprogrammes ermöglicht wurde.

AVANT-PROPOS

Lors d'études de concepts d'évacuation de déchets radioactifs dans des formations géologiques, on attache une grande importance à l'acquisition d'informations étendues sur la roche d'accueil et les formations rocheuses environnantes. C'est pour cette raison que la Cédra exploite depuis mai 1984 son **Laboratoire souterrain du Grimsel (LSG)** situé à 450 m de profondeur dans les roches cristallines du massif de l'Aar, situé au centre des Alpes suisses. Les principaux objectifs des recherches effectuées dans ce laboratoire concernent

- l'acquisition de savoir-faire dans diverses disciplines techniques et scientifiques pour la conception, la réalisation et l'interprétation d'expériences dans le terrain et

- la récolte d'expériences pratiques dans la mise au point de méthodologies d'investigation, de techniques de mesure et avec les appareillages qui pourraient être utilisés lors de l'exploration de sites potentiels de dépôts finals.

Le LSG est exploité par la Cédra et diverses expériences y sont réalisées par celle-ci et deux Institutions allemandes, la "Bundesanstalt für Geowissenschaften und Rohstoffe, Hannover" (BGR) et le "Forschungszentrum für Umwelt und Gesundheit GmbH, München" (GSF) dans le cadre d'un traité de collaboration germano-suisse. Les projets poursuivis au Grimsel par la BGR et le GSF sont supportés par le Ministère fédéral allemand de la recherche et de la technologie (BMFT). Les rapports NTB 85-46 (version anglaise) et NTB 85-47 (version allemande) présentent un aperçu du laboratoire souterrain et un résumé des programmes de recherches. La situation de ce programme en 1988 est présentée dans la publication "Cédra informe 1+2/1988" (version française) et "Nagra informiert 1+2/1988" (version allemande) ainsi que dans une édition spéciale en anglais (Nagra Bulletin 1988).

L'**expérience de migration de radionucléides (MI)** représente une contribution majeure de la Cédra au programme du Grimsel. MI est une étude multidisciplinaire ayant pour objectif l'étude du transport en solution dans des milieux rocheux fracturés. Les travaux de terrain sont supportés par un programme de modélisation hydrodynamique, chimique et de transport, complétés par des essais en laboratoire. Ce projet qui a débuté en 1985 et devrait se terminer en 1994, fut initialement conçu comme une collaboration entre la Cédra et l'Institut Paul Scherrer (IPS). Depuis 1987 des essais de terrain avec des traceurs radioactifs ont été réalisés avec l'Institut d'hydrogéologie de la GSF de Münich-Neuherberg. En 1989 un accord bilatéral de collaboration a été signé avec la Power Reactor and Nuclear Fuel Development Corporation (PNC) de Japon qui a conduit à une extension substancielle du Projet de migration de radionucléides au Grimsel.

Le présent rapport a été élaboré dans le cadre des accords de collaboration mentionnés. Les auteurs ont présenté leurs vues et conclusions personnelles. Celles-ci ne doivent pas forcément correspondre à celles de Nagra ou ses partenaires participants.

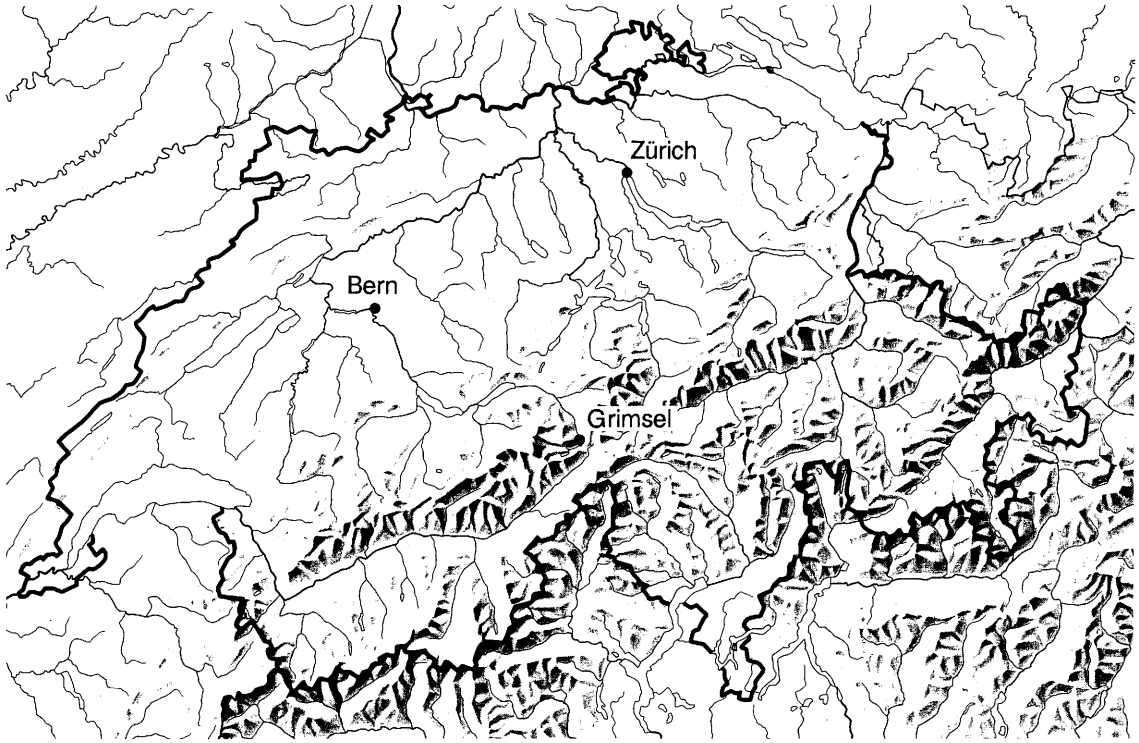

Location of Nagra's underground test facility at the Grimsel Pass in the Central Alps (Bernese Alps) of Switzerland (approximate scale 1 cm = 25 km).

Geographische Lage des Nagra Felslabors am Grimselpass (Berner Oberland) in den schweizerischen Zentralalpen (Massstab: 1 cm = ca. 25 km)

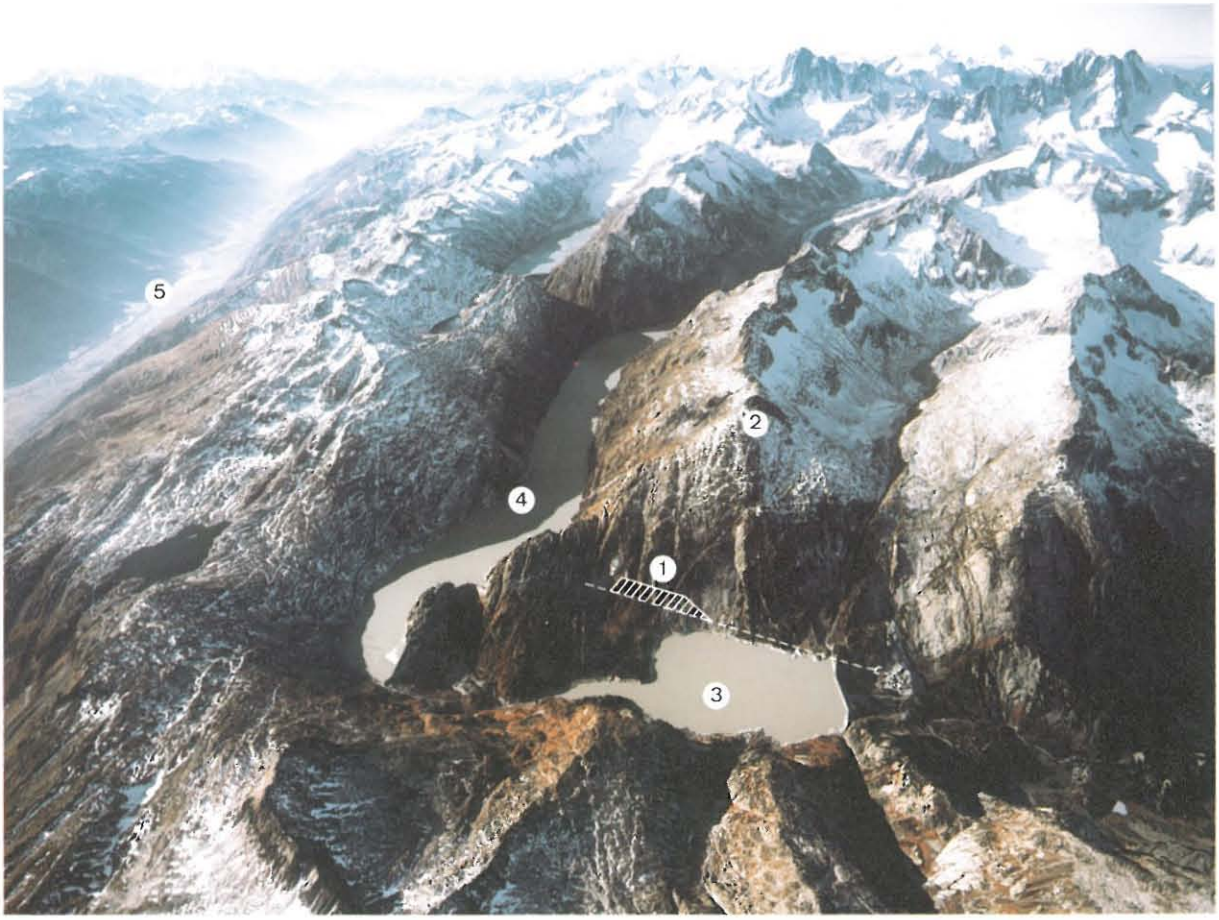

GRIMSEL-GEBIET

Blick nach Westen

1 Felslabor
2 Juchlistock
3 Räterichsbodensee
4 Grimselsee
5 Rhonetal

GRIMSEL AREA

View looking West

1 Test Site
2 Juchlistock
3 Lake Raeterichsboden
4 Lake Grimsel
5 Rhone Valley

FLG FELSLABOR GRIMSEL
GTS *GRIMSEL TEST SITE*

Situation

0 100 m

- Zugangsstollen/*Access tunnel*
- Fräsvortrieb/*by tunnel boring machine*
- Sprengvortrieb/*excavated by blasting*
- Zentraler Aaregranit ZAGR / *Central Aaregranite CAGR*
- Biotitreicher ZAGR / *CAGR with high content of biotite*
- Grimsel-Granodiorit / *Grimsel-Granodiorite*
- Scherzone/*Shear zone*
- Lamprophyr/*Lamprophyre*
- Wasserzutritt/*Water inflow*
- SB Sondierbohrung/*Exploratory borehole*
- US US Bohrung/*US borehole*

ZB	Zentraler Bereich/*Central facilities*
AU	Auflockerung/*Excavation effects*
BK	Bohrlochkranz/*Fracture system flow*
EM	El.magn. HF-Messungen/*-measurements*
FRI	Kluftzone/*Fracture zone investigation*
GS	Gebirgsspannungen/*Rock stresses*
HPA	Hydr. Parameter/*Hydr. parameters*
MI	Migration/*Migration*
MOD	Hydrodyn. Modellierung/*H. modeling*
NM	Neigungsmesser/*Tiltmeters*
UR	Untertageradar/*Underground radar*
US	Seismik/*Underground seismic testing*
VE	Ventilationstest/*Ventilation test*
WT	Wärmeversuch/*Heat test*

A — A Schnitt/*Section*

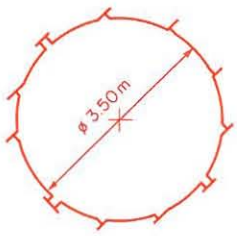

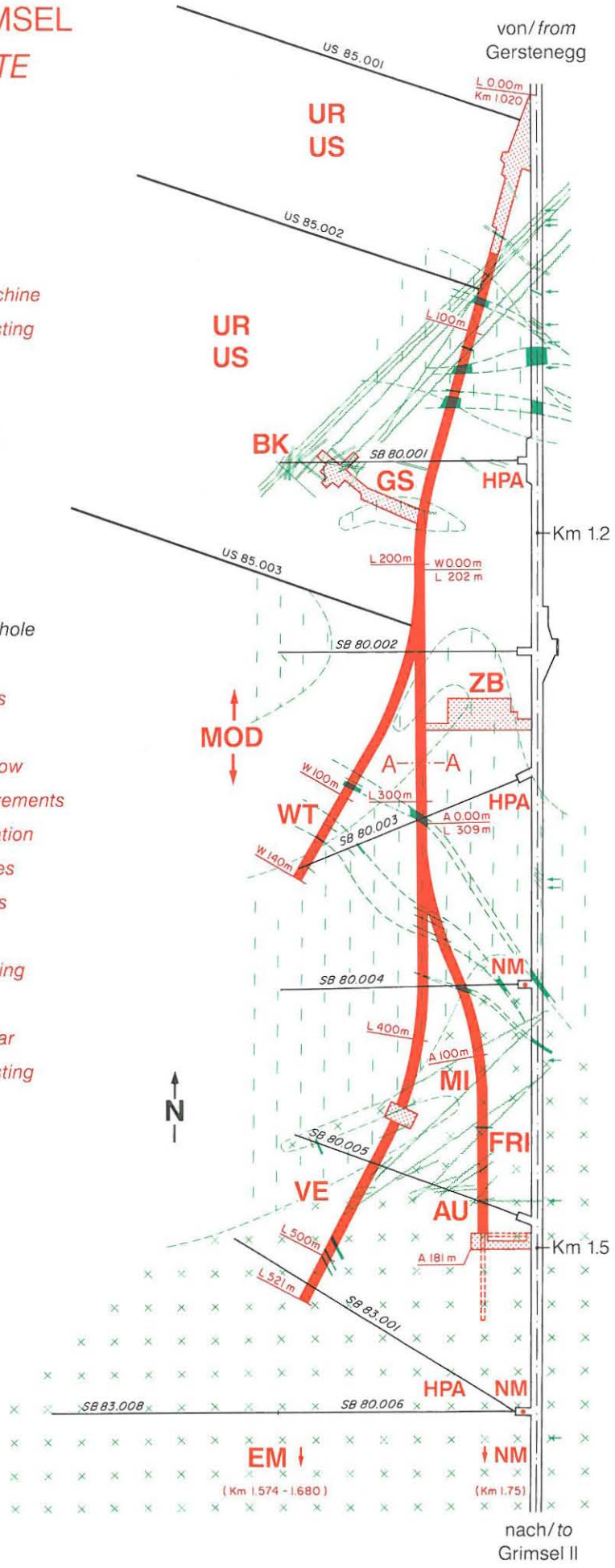

6/88

Preface

In the framework of its Waste Management Programme the Paul Scherrer Institute is performing work to increase the understanding of the migration behavior of nuclear waste relevant radionuclides. These investigations are performed in close cooperation with, and with the financial support of NAGRA. The present report is issued simultaneously as a PSI report and a NAGRA report.

Contents

Abstract

To understand the results of the field migration experiments of NAGRA at the Grimsel Test Site (Central Switzerland), it is necessary to develop models (hydraulic as well as transport models). In this paper a simple approach with streamtubes is described which allows to model the hydraulic situation for asymmetric dipole arrangements and transport along streamlines, including sorption and diffusion into fracture infill material. The model is confronted with two experiments, one with a nonsorbing tracer (uranine) and the other with sorbing (^{24}Na) and nonsorbing tracer material. The fit-by-eye parameter values are compatible with those from batch experiments. The sensitivity of breaktrough curves on the chosen parameters was checked with a parameter variation study. In the range of considered variations the breakthrough curves of non-sorbing tracers are not sensitive to matrix properties because saturation is achieved in all the cases considered. For sorbing tracers the situation is more complicated as saturation may be achieved or not within the experimental timescale; due to this fact, it is emphasized, that step input experiments should be performed instead of pulse test experiments.

Résumé

Afin de comprendre les essais de migration de la CEDRA au "Felslabor Grimsel", il faut confronter l'expérience aux modèles. Dans ce rapport, un modèle est proposé avec les charactéristiques suivantes: i) la domaine d'écoulement entre l'injection et l'extraction (dipôle asymmétrique) est divisé sur le périmètre d'essai en "tubes" d'écoulement. ii) Un transport advectif et unidimensionnel a lieu en chaque "tube" d'écoulement. iii) Perpendiculairement au plan d'écoulement, la diffusion a lieu dans la matière de remplissage de la fissure. Selon traçeur utilisé, la diffusion peut être accompagnée d'une sorption. iv) La distribution des concentrations avec le temps complète au point d'extraction est la somme des distributions pour chaque tube d'écoulement corrigé pour son débit relatif.

Ce modèle a été utilisé pour l'interpretation de deux essais. Les paramètres du modèle sont en accord avec les résultats des essais de laboratoire (sorption en "batch"). Pour évaluer la sensibilité du modèle, des calculs sont réalisés avec les paramètres. Pour les variations des paramètres choisis, l'étude conduit aux conclusions suivantes: La diffusion dans la matrice (mieux: la diffusion dans la matière de remplissage de la fissure) ne peut être identifiée sans ambiguité dans le cas des traçeurs non-sorbants, tandis que pour des traçeurs sorbants, elle doit être prise en considération, dans les domaines choisis des paramètres. Ici, la situation plus complexe induit la question: "La matière de remplissage de la fissure, est-elle saturée durant les essais, ou non?"

Zusammenfassung

Um die Migrationsexperimente der NAGRA, die zur Zeit im Felslabor Grimsel im Gange sind, verstehen zu können, müssen die Experimente Modellvorstellungen gegenübergestellt werden: in diesem Bericht wird ein Transportmodell mit folgenden Charakteristiken vorgestellt: i) Das zugrunde liegende Fliessfeld zwischen input und output (asymmetrischer Dipol) wurde flächendeckend in Stromröhren unterteilt. ii) In jeder Stromröhre findet eindimensionaler, advektiver Transport statt. iii) Senkrecht zur Fliessebene findet Diffusion in die Kluftfüllung statt; diese Diffusion wird tracerabhängig durch Sorption eventuell retardiert. iv) Die Durchbruchskurve am Beobachtungsort ist eine mit den entsprechenden Fliessraten gewichtete Ueberlagerung der einzelnen Durchbruchskurven aller Stromröhren.

Dieses Modell wurde zur Interpretation zweier Versuche verwendet; die daraus resultierenden Fitparameters sind im Einklang mit entsprechenden experimentellen Werten aus Batch–Versuchen. Um die Empfindlichkeit der Resultate gegenüber Parameterschwankungen zu untersuchen, wurde eine Parameter–Variations–Studie durchgeführt, die im Rahmen der gewählten Parameterbereiche zu folgenden Folgerungen führten: Mit nicht–sorbierenden Tracern kann Matrixdiffusion (besser: Diffusion in Kluftfüllung) nicht eindeutig identifiziert werden, währenddem dies für den Fall sorbierender Tracer in einzelnen Parameterbereichen als möglich erscheint; hier wird die Situation durch die Frage "Sättigung der Kluftfüllung innerhalb der experimentellen Zeiten: ja oder nein?" erschwert.

1 Introduction

At the Grimsel Test Site (GTS) of NAGRA in central Switzerland, migration experiments with conservative and sorbing tracers are conducted. The goal of these experiments is to test our understanding of transport mechanisms on a scale larger than that of laboratory experiments, i.e. a few meters in the field versus a few centimeters in the laboratory. To achieve such an understanding, a close collaboration between experimentalists and modellers is a condition for an iterative approach to data interpretation. It is, therefore, important that modellers advise experimentalists in the layout of the experiment: on the basis of predictions, calibrated on earlier experiments, they should propose the arrangements in which transport parameters can be extracted with minimal ambiguity. In this report, a simple transport model is presented; firstly, it allows to understand experimental results within the framework of dual porosity models and secondly, predictions for future experiments can be made.

No attempts were made to interpret "double peak" breakthrough curves because the shape of such curves is apparently very strongly dependent on the experimental setup; also, the complexity of these breakthrough curves exceeds the framework of the model presented here.

2 The streamtube approach

To model transport at the Grimsel Test Site (GTS), the hydrology of a certain experimental setup has to be known as accurately as possible. Therefore, a number of hydraulic tests has been performed [1]; these tests were the basics for a hydraulic model where the migration fracture was considered as a 2D equivalent porous, isotropic and heterogeneous aquifer [2]. This model generates a velocity field $\vec{q}(x,y)$ that, in principle, can be used as input for a 2D transport model. Not yet resolved numerical problems on one side and the need for transport predictions for experiments with ^{22}Na and ^{85}Sr on the other, made the development of a simple transport model unavoidable. This simple model is outlined in this and the following section.

The preliminary migration tests ("Vorversuche") were performed as unequal dipole experiments between the boreholes 4/6, 4/9, 9/6. (For a review of the migration site and the nomenclature of the boreholes see e.g. [1], [2]) Under non–stress conditions (i.e. all boreholes sealed) it is an experimental fact that in the region of these boreholes (4, 6, 9) the hydraulic head is very flat (head differences of a few centimeters for a total head of about 12 m); the interpretation could be that the heterogeneities somehow compensate the drainage effect of the laboratory drift (see e.g. [2], Fig. 9a). Due to this apparent homogeneity, the hydrology of an unequal dipole experiment in this area can be described via superposition of hydraulic heads of a pumping well of strength Q_w and an injection well of strength Q_i.

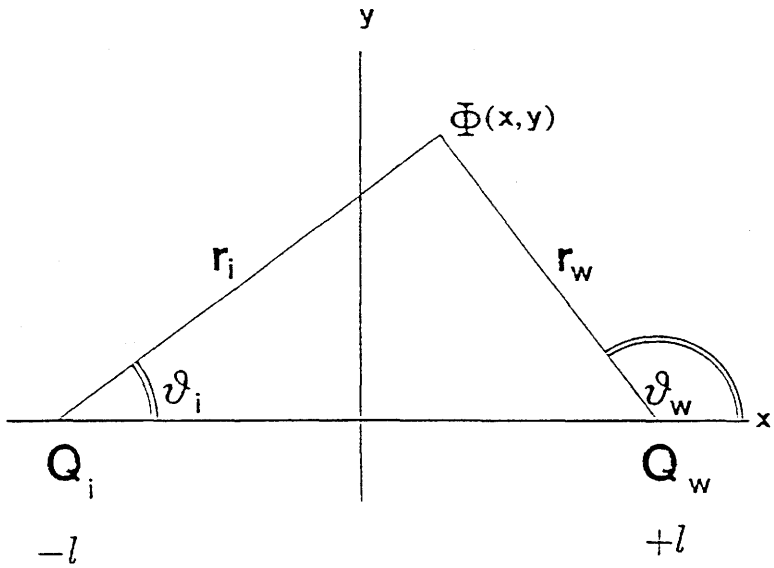

Figure 1: The geometry for a dipole arrangement

Mathematically, this means

$$\Phi(x,y) = \Phi_\circ + \frac{Q_w}{4\pi T} ln \frac{r_w^2}{r_\circ^2} - \frac{Q_i}{4\pi T} ln \frac{r_i^2}{r_\circ^2} \tag{1}$$

$\Phi(x,y)$	:	hydraulic head at location (x,y)
$\Phi_\circ$	:	arbitrary constant to define the horizon
T	:	mean transmissivity of the aquifer
$r_\circ$	:	radius of the borehole
$Q_{w,i}$	:	withdrawal/injection rate at borehole

The distances r_w, r_i are given by

$$r_i^2 = (l+x)^2 + y^2 \tag{2a}$$

$$r_w^2 = (l-x)^2 + y^2 \tag{2b}$$

where $2l$ is the distance between the injection and pumping well (see Fig. 1). Due to Darcy's law the components of the discharge vector $\vec{q} = (q_x, q_y)$ are given by

$$q_x = -\frac{T}{a}\frac{\partial \Phi}{\partial x} = \frac{Q_i}{2\pi a}\left\{\frac{(l+x)}{(l+x)^2+y^2} + \beta\frac{(l-x)}{(l-x)^2+y^2}\right\} \tag{3a}$$

$$q_y = -\frac{T}{a}\frac{\partial \Phi}{\partial y} = \frac{Q_i}{2\pi a}\left\{\frac{y}{(l+x)^2+y^2} - \beta\frac{y}{(l-x)^2+y^2}\right\} \tag{3a}$$

Here a is the width of the aquifer, assumed to be constant, and β is defined as

$$\beta = \frac{Q_w}{Q_i}$$

To improve the chance for 100% tracer recovery, only the case $\beta \geq 1$ will be discussed.

$\Phi(x,y)$ of eq. (1) is the solution of the Laplace equation in two dimensions

$$\Delta\Phi(x,y) \equiv \frac{\partial^2\Phi}{\partial x^2} + \frac{\partial^2\Phi}{\partial y^2} = 0 \tag{4a}$$

with the boundary condition at some distant location R

$$-2\pi r T \left.\frac{\partial \Phi}{\partial r}\right|_{r=R} = Q_i - Q_w \tag{4b}$$

Eq. (4a) is the basic equation for the two–dimensional potential theory. From this theory, there exists a so called stream function Ψ such that

$$\Omega = \frac{T}{a}\Phi + i\Psi$$

is an analytical function. This implies that the Cauchy–Riemann relations hold between the real and imaginary part [3]:

$$\frac{T}{a}\frac{\partial\Phi}{\partial x} = \frac{\partial\Psi}{\partial y} \tag{5a}$$

$$\frac{T}{a}\frac{\partial\Phi}{\partial y} = -\frac{\partial\Psi}{\partial x} \tag{5b}$$

With help of eq. (3) and eq. (5) the stream function Ψ can be calculated for the unequal dipole case under study:

$$\begin{aligned}\Psi(x,y) &= \frac{Q_i}{2\pi a}\left\{arcsin\frac{x+l}{\sqrt{(x+l)^2+y^2}} - \beta\ arcsin\frac{x-l}{\sqrt{(x-l)^2+y^2}} + c_1\right\} \\ &= \frac{Q_i}{2\pi a}\left\{-\vartheta_i + \beta\vartheta_w + (1-\beta)\frac{\pi}{2} + c_1\right\}\end{aligned}$$

The angles, ϑ_i and ϑ_w are shown in Fig. 1. The integration constant c_1 is arbitrary; for this study it will be fixed such that $\Psi = 0$ for $y = 0, -l \leq x \leq +l$ (i.e. $\vartheta_i = 0, \vartheta_w = \pi$):

$$c_1 = -(1+\beta)\frac{\pi}{2}$$

This yields

$$\Psi(x,y) = \frac{Q_i}{2\pi a}\left\{arcsin\frac{x+l}{\sqrt{(x+l)^2+y^2}} - \beta\ arcsin\frac{x-l}{\sqrt{(x-l)^2+y^2}} - \frac{1}{2}(1+\beta)\pi\right\} \tag{6a}$$

$$= \frac{Q_i}{2\pi a}\left\{-\vartheta_i + \beta\vartheta_w - \beta\pi\right\} \tag{6b}$$

As the x–axis is a symmetry axis of the problem, it suffices to discuss any properties in e.g. the upper half plane ($y \geq 0$). The range of values the stream function can have is given by:

$$\vartheta_i = 0, \vartheta_w = \pi \quad : \quad \Psi = 0 \tag{7a}$$

$$\vartheta_i = \pi, \vartheta_w = \pi \quad : \quad \Psi = -\tfrac{1}{2}(Q_i/a) \tag{7b}$$

$$\vartheta_i = 0, \vartheta_w = 0 \quad : \quad \Psi = -\tfrac{1}{2}(Q_w/a) \tag{7c}$$

Two properties of the stream function Ψ are crucial for the development of the approach chosen in that report:

(i) The path a water molecule is travelling along (the so called streamline) with a velocity $\vec{q}$ is defined by the alignment of $\vec{q}$ and the line element $d\vec{s}$:

$$\vec{q} \times d\vec{s} = 0$$

With help of eqs. (3) and eqs. (5) one gets:

$$\begin{aligned} \vec{q} \times d\vec{s} &= \left(-\frac{T}{a}\frac{\partial\Phi}{\partial x}\vec{i} - \frac{T}{a}\frac{\partial\Phi}{\partial y}\vec{j}\right) \times (dx\vec{i} + dy\vec{j}) = -\frac{T}{a}\left(\frac{\partial\Phi}{\partial x}dy - \frac{\partial\Phi}{\partial y}dx\right)\vec{k} \\ &= -\left(\frac{\partial\Psi}{\partial y}dy + \frac{\partial\Psi}{\partial x}dx\right)\vec{k} = -d\Psi\vec{k} = 0 \end{aligned}$$

$\vec{i}$, $\vec{j}$ and $\vec{k}$ are the usual linearly independent unit vectors.

This means that the stream function Ψ is constant along a streamline.

(ii) Consider the flow (rate Q) through an area A of an aquifer of thickness a, as shown in Fig. 2:

$$\begin{aligned} Q = \int \vec{q} \cdot d\vec{A} &= a\int_1^2 \vec{q}(d\vec{l} \times \vec{k}) = a\int_1^2 (\vec{q} \times d\vec{l}) \cdot \vec{k} \\ &= -a\int_1^2 d\Psi = a(\Psi_1 - \Psi_2) \end{aligned} \tag{8}$$

The flowrate through a region bound by two planes of constant stream functions is given by the product of aquifer thickness and the difference of the stream functions; a region between planes of constant stream functions and thickness a is thus called a <u>streamtube.</u>

Apart from these two properties the length of a certain streamline and the transit time along it is of importance for the transport model to be presented in the next paragraph. For this purpose the streamline $y(x)$ has to be determined through the implicit eq. (6) where $\Psi(x,y)$ is a constant in the range given by eqs. (7). In general, a streamline $y(x)$ has a shape as shown in Fig.3:

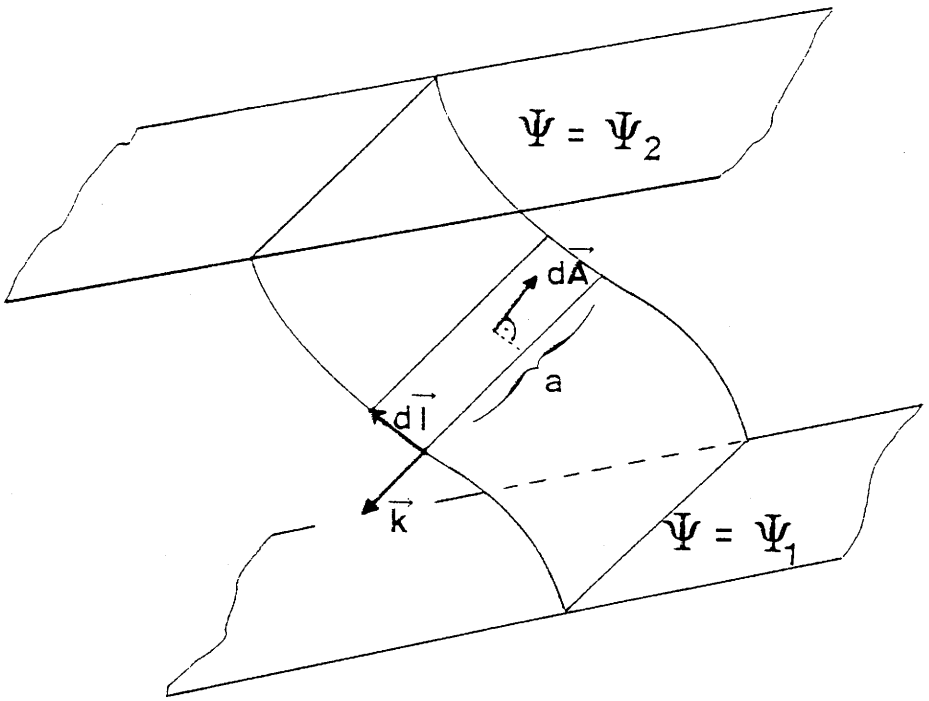

Figure 2: Flow through a streamtube

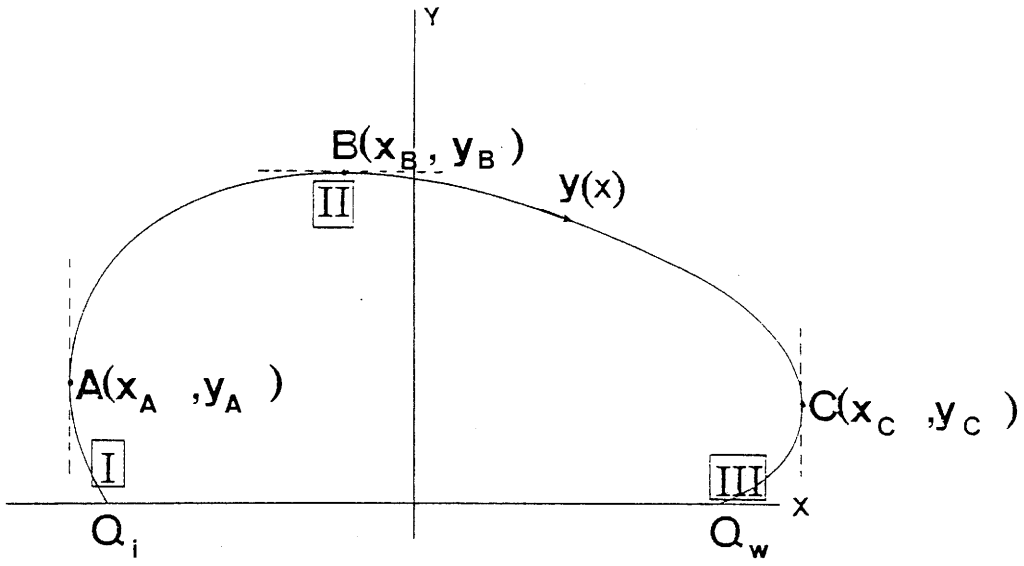

Figure 3: Characteristic points of a streamline

There are three characteristic points:

(i) the two turning points A = (x_A, y_A) and C = (x_C, y_C). At these points the velocity has only a y–component, thus $q_x \mid_{A,C} = 0$.

(ii) the point B = (x_B, y_B) where the velocity has only a x–component, $q_y \mid_B = 0$.

The turning points A and C occur only for $\Psi \geq \Psi_{crit}$ and it is always true that $x_A \leq -l, x_C \geq +l$. As a consequence segment I and segment III only occur for streamlines with $\Psi > \Psi_{crit}$. The values for Ψ_{crit} will be given below.

Computation of B = (x_B, y_B)

From $q_y \mid_B = 0$ it follows:

$$y^2 = \frac{(x-l)^2 - \beta(l+x)^2}{\beta - 1} \tag{9a}$$

Inserted into the implicit equation (6a) for the streamline this yields

$$\phi = \beta \; arcsin\sqrt{\frac{\beta-1}{\beta}}\frac{x-l}{2\sqrt{-xl}} - arcsin\sqrt{\beta-1}\frac{x+l}{2\sqrt{-xl}} \tag{9b}$$

where

$$\phi = -\frac{2\pi a}{Q_i}\Psi - \frac{\pi}{2}(1+\beta) = C - \frac{\pi}{2}(1+\beta) \tag{9c}$$

$$C = -\frac{2\pi a}{Q_i}\Psi \quad , \quad C\epsilon[0, \beta\pi] \tag{9d}$$

Eq. (9b) has to be solved numerically for $x = x_B$. The solution x_B has to be looked for in a certain range, given by the following conditions.

i) from (9a) : $\dfrac{(x-l)^2 - \beta(l+x)^2}{\beta - 1} \geq 0$

ii) from (9b) : $\left|\sqrt{\dfrac{\beta-1}{\beta}}\dfrac{x-l}{2\sqrt{-xl}}\right| \leq 1 \quad ; \left|\sqrt{\beta-1}\dfrac{x+l}{2\sqrt{-xl}}\right| \leq 1$

This yields

$$(x_B)_{min} = -l\frac{(1+\sqrt{\beta})^2}{\beta-1} \leq x_B \leq -l\frac{(1-\sqrt{\beta})^2}{\beta-1} = (x_B)_{max} \tag{9e}$$

Introducing

$$f_B = \phi - \beta \; arcsin\sqrt{\frac{\beta-1}{\beta}}\frac{x-l}{2\sqrt{-xl}} + arcsin\sqrt{\beta-1}\frac{x+l}{2\sqrt{-xl}}$$

one finds

$$f_B(x = (x_B)_{min}) = C - \pi$$

$$f_B(x = (x_B)_{max}) = C$$

and therefore eq. (9b) has a unique solution only if:

$$f_B(x = (x_B)_{min}) \cdot f_B(x = (x_B)_{max}) \leq 0 \quad : \quad C(C-\pi) \leq 0 \quad : \quad C \leq \pi$$

Therefore the extremum B = (x_B, y_B) exists only for those streamlines that fulfill

$$0 \geq \Psi \geq -\frac{Q_i}{2a} \tag{9f}$$

In the case of an equal dipole ($\beta = 1$) x_B, y_B can be given analytically

$\beta = 1$: $\qquad x_B = 0(\text{symmetry!})$

$$y_B = l(1 - cosC)/sinC$$

In addition, in this case all the streamlines have an extremum B.

Computation of A = (x_A, y_A) and C = (x_C, y_C)

From $q_x \mid_{A,C} = 0$ it follows:

$$y^2 = (x^2 - l^2)\frac{(l-x) + \beta(l+x)}{\beta(l-x) + (l+x)} \tag{10a}$$

Inserted into eq. (6a) yields

$$\phi = \beta\ arcsin\left\{(x-l)\sqrt{\frac{\beta(l-x)+l+x}{4\beta x l(x-l)}}\right\} - arcsin\left\{(x+l)\sqrt{\frac{\beta(l-x)+l+x}{4xl(x+l)}}\right\} \tag{10b}$$

The solutions x_A, x_C of this equation have to be found numerically. The range in which these solutions can be found can be calculated in analogy to the former calculation done for B = (x_B, y_B):

$$(x_A)_{min} = -l\frac{\beta+1}{\beta-1} \leq x_A \leq -l = (x_A)_{max} \tag{10c}$$

$$(x_C)_{min} = +l \leq x_C \leq l\frac{\beta+1}{\beta-1} = (x_C)_{max} \tag{10d}$$

With

$$f_{ext} = \phi - \beta\ arcsin\left\{(x-l)\sqrt{\frac{\beta(l-x)+(l+x)}{4\beta x l(x-l)}}\right\} + arcsin\left\{(x+l)\sqrt{\frac{\beta(l-x)+l+x}{4xl(x+l)}}\right\} \tag{10e}$$

one finds

$$f_{ext}\,(x = (x_A)_{min}) = C - \pi$$

$$f_{ext}\,(x = (x_A)_{max}) = C - \frac{\pi}{2}$$

on one side and

$$f_{ext}\,(x = (x_C)_{min}) \;\; = C - \beta\frac{\pi}{2}$$
$$f_{ext}\,(x = (x_C)_{max}) \;\; = C - (1+\beta)\frac{\pi}{2}$$

on the other side.

Eq. (10b) allows for a turning point A = (x_A, y_A) if

$$f_{ext}\,(x = (x_A)_{min}) \cdot f_{ext}\,(x = (x_A)_{max}) \;\; \leq \;\; 0 \qquad : \quad (C-\pi)\cdot\left(C - \frac{\pi}{2}\right) \leq 0$$

and a turning point C = (x_C, y_C) exists if

$$f_{ext}(x = (x_C)_{min}) \cdot f_{ext}\,(x = (x_C)_{max}) \;\; \leq \;\; 0 \qquad : \left(C - \beta\frac{\pi}{2}\right)\left(C - (1+\beta)\frac{\pi}{2}\right) \leq 0$$

Therefore a turning point A = (x_A, y_A) exists only for those streamlines whose stream function is in the following range.

$$\text{turning point A:} \quad -\frac{Q_i}{2a} \leq \Psi \leq -\frac{Q_i}{4a} \tag{10f}$$

Similarly for turning point C:

$$\text{turning point C:} \quad -(1+\beta)\frac{Q_i}{4a} \leq \Psi \leq -\beta\frac{Q_i}{4a} \tag{10g}$$

The bounds in eqs. (10f), (10g) are the critical values Ψ_{crit} mentioned after Fig. 3.

In case of an equal dipole $x_A = -x_C, y_A = y_C$ can be given explicitly:

$$\beta = 1 \qquad : \quad x_C = -x_A = \frac{l}{sinC} \qquad : \quad \tfrac{\pi}{2} \leq C \leq \pi$$
$$y_C = y_A = -\frac{lcosC}{sinC}$$

Computation of the streamline

With the knowledge of the points A, B and C mentioned above the streamlines $y(x)$ can be calculated in a straightforward way from eq. (6a)

$0 \leq C \leq \pi$: For these values of C there exists for each $x\epsilon[-l,+l]$ a unique solution $y_c(x)$ of eq. (6a) with
$0 \leq y_c(x) \leq y_B$

$x \leq 0 : \frac{\pi}{2} \leq C \leq \pi$: For these values of C there exist for each $x\epsilon[x_A,-l]$ two solutions $y_1(x), y_2(x)$ of eq (6a) with
$0 \leq y_1(x) \leq y_A$
$y_A \leq y_2(x) \leq y_B$

$x \geq 0 : \beta\frac{\pi}{2} \leq C \leq (\beta+1)\frac{\pi}{2}$: For these values of C there exist for each $x\epsilon[l,x_C]$ two solutions $y_3(x), y_4(x)$ of eq. (6a) with
$y_C \leq y_3(x) \leq y_B$
$0 \leq y_4(x) \leq y_C$

For the equal dipole case ($\beta = 1$) the streamline $y(x)$ can be given explicitly:

$$\beta = 1 : \; y(x) = \left\{ \begin{array}{ll} \dfrac{-lcosC + \sqrt{l^2 - x^2 sin^2 C}}{sinC} & = y_c \\ \dfrac{-lcosC + \sqrt{l^2 - x^2 sin^2 C}}{sinC} & = y_2 = y_3 \\ \dfrac{-lcosC - \sqrt{l^2 - x^2 sin^2 C}}{sinC} & = y_1 = y_4 \end{array} \right\} \quad \begin{array}{l} \mid x \mid \leq l, \quad 0 \leq C \leq \pi \\ l \leq \mid x \mid \leq \dfrac{l}{sinC}, \dfrac{\pi}{2} \leq C \leq \pi \end{array}$$

The length of a streamline

The arc length of an arbitrary curve between x_1 and x_2 is given by

$$L = \int_{x_1}^{x_2} ds = \int_{x_1}^{x_2} \sqrt{dx^2 + dy^2} = \int_{x_1}^{x_2} dx \sqrt{1 + (y'(x))^2}$$

and therefore the length of a streamline between injection and withdrawal hole is given by

$$\begin{aligned} L = \; & \Theta(C - \frac{\pi}{2}) \int_{x_A}^{-l} dx \left(\sqrt{1 + (y_1'(x))^2} + \sqrt{1 + (y_2'(x))^2} \right) + \int_{-l}^{+l} dx \sqrt{1 + (y_c'(x))^2} \\ & + \Theta(C - \beta\frac{\pi}{2}) \int_{l}^{x_C} dx \left(\sqrt{1 + (y_3'(x))^2} + \sqrt{1 + (y_4'(x))^2} \right) \quad , \Theta(t) = \left\{ \begin{array}{ll} 1 & t > 0 \\ 0 & t < 0 \end{array} \right. \end{aligned} \tag{11a}$$

Remember, only streamlines with $C \leq \pi$ link the injection and the withdrawal hole.

For $\beta = 1$ the integrals of eq. (11) can be performed analytically since the streamline $y(x)$ is known explicitly:

$$\beta = 1 \qquad L = 2l\frac{C}{sinC} = L_o\frac{C}{sinC} \quad , L_o = 2l \qquad , C\epsilon[0,\pi] \tag{11b}$$

The transit time along a streamline

The transit time along an arbitrary curve between x_1 and x_2 is given by

$$T_t = \int_{x_1}^{x_2} \frac{ds}{v} = \int_{x_1}^{x_2} \frac{dx\sqrt{1+(y'(x))^2}}{\sqrt{v_x^2+v_y^2}}$$

For the streamline $\vec{q}$ x $d\vec{s} = 0$ a differential equation can be derived:

$$\vec{q} \text{ x } d\vec{s} = q_x dy - q_y dx = 0 : \frac{dy}{dx} = \frac{q_y}{q_x} = \frac{v_y}{v_x}$$

and therefore

$$\sqrt{v_x^2+v_y^2} = \mid v_x \mid \sqrt{1+\left(\frac{v_y}{v_x}\right)^2} = \mid v_x \mid \sqrt{1+(y'(x))^2}$$

Thus the transit time along a streamline connecting the input and withdrawal well (i.e. $C \leq \pi$) is given by ($q_x = \epsilon v_x, \epsilon$: connected porosity)

$$\begin{aligned} T_t = \epsilon \; & \left\{ \Theta(C-\frac{\pi}{2}) \int_{x_A}^{-l} dx \left\{ \frac{1}{\mid q_x \mid}\bigg|_{y=y_1(x)} + \frac{1}{\mid q_x \mid}\bigg|_{y=y_2(x)} \right\} + \int_{-l}^{+l} dx \; \frac{1}{\mid q_x \mid}\bigg|_{y=y_c(x)} \right. \\ + \; & \left. \Theta(C-\beta\frac{\pi}{2}) \int_{l}^{x_C} dx \left\{ \frac{1}{\mid q_x \mid}\bigg|_{y=y_3(x)} + \frac{1}{\mid q_x \mid}\bigg|_{y=y_4(x)} \right\} \right\} \end{aligned} \tag{12a}$$

For the equal dipole ($\beta = 1$) eq. (12a) takes the following form:

$$\beta = 1 \qquad T_t = \frac{4\pi a\epsilon}{Q_i}\frac{l^2}{sin^2 C}(1 - CctgC) \qquad C\epsilon[0,\pi] \tag{12b}$$

Eq. (12a) can also be given explicitly for the streamline $y(x) = 0$ for any β [4]:

$$y(x) = 0 : \qquad T_o = T_t|_{y=0} = \frac{4\pi a\epsilon}{Q_i}\frac{l^2}{\beta-1}\left\{\frac{\beta+1}{\beta-1} - \frac{2\beta}{(\beta-1)^2} ln\beta\right\} \tag{13}$$

For convenience, the most important results and its implications will be summarized below:

i) A streamtube is defined as the volume given by the aquifer thickness a times the area between streamlines, characterized by the stream functions Ψ_i and Ψ_k. The flowrate Q_{ik} through such a streamtube is given by $Q_{ik} = a \mid \Psi_i - \Psi_k \mid$ (see Fig. 2).

ii) All the streamlines starting at the injection hole are characterized by stream functions out of the interval $C\epsilon[0, \pi], \Psi = -(Q_i/2\pi a)C$; they all end at the withdrawal hole (this is valid for $\beta = Q_w/Q_i \geq 1$, the case considered in this report). This observation is a consequence of eq. (7b) and eq. (10f).

iii) All the streamlines which are characterized by stream functions out of the interval $C\epsilon(\pi, \beta\pi)$, $\Psi = -(Q_i/2\pi a)C$ start at the outer boundary of the streamtube and end at the withdrawal hole; this of course is a consequence of the boundary condition eq. (4b). This implies that tracer arriving from the injection hole at the withdrawal hole will be diluted by the ratio Q_i/Q_w.

3 The transport model

Based on the results of the previous section the concept of the transport model is as follows:

i) the transport of tracer from the input well to the withdrawal hole is taking place along streamtubes; this is modelled in a one–dimensional way (neglecting matrix diffusion for the moment): The tracer moves along a streamline y_k of a certain length L_k (its length being in the range between the lengths of the streamlines defining the streamtube k) with a certain average velocity $\overline{v}_k$ defined as $\overline{v}_k = L_k/T_k$ where T_k is the transit time along streamline y_k. This is schematically depicted in Figure 4.

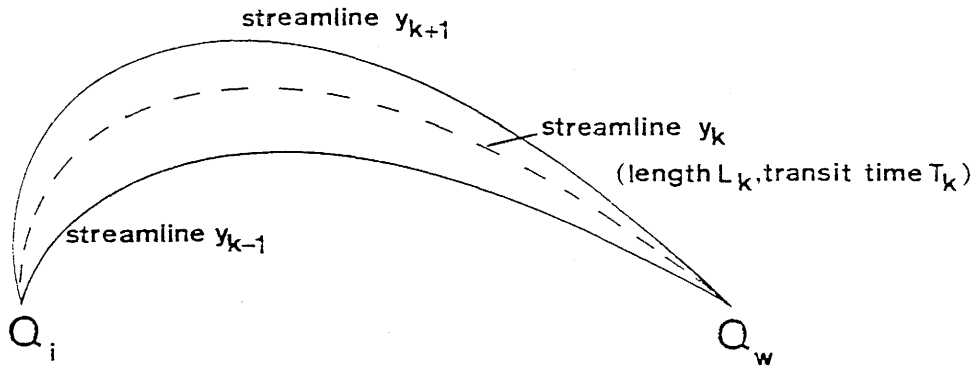

Figure 4: The streamtube k and quantities used in the transport model

ii) the breakthrough curve at the withdrawal hole is a result of the superposition of all the streamtube contributions $C^{(k)}$ ($C^{(k)}$: concentration of tracer in streamtube k) weighted with the appropriate flowrate percentage in that streamtube k. The dilution factor mentioned in the summary of the former section multiplies this superposition sum:

$$C(x=+l, y=0) = 2\frac{Q_i}{Q_w}\sum_{k=1}^{m}\left\{\frac{\mid a(\Psi_k - \Psi_{k-1})\mid}{Q_i} C^{(k)}(x=+l, y=0)\right\} \qquad (14)$$

To cover the whole flowfield Ψ_o and Ψ_m have to be: $\Psi_o = 0$, $\Psi_m = -Q_i/(2a)$. The factor of two in eq. (14) takes care of the fact that the contribution from the ($y < 0$) half plane is equally contributing as the one from the ($y > 0$) half plane. The number m in eq. (14) can be chosen arbitrarily; it is determined by the resolution the final breakthrough curve should have in comparison to the experimental curve.

iii) the fracture AU96m of width a has a porous infill. The flow–porosity ϵ_f is thought to be made out of n plane parallel open fractures of halfwidth b and matrix (thickness 2D)in between; this is visualized in Fig. 5:

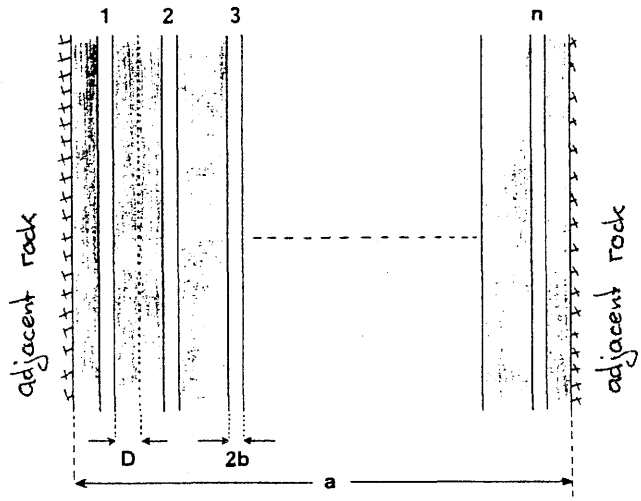

Figure 5: Modelling the geometry of the infill in the migration fracture AU96m

With this picture of the migration fracture advective transport takes place along n open fractures (of width 2b) and diffusion perpendicular to these fractures into the infill–matrix (with porosity ϵ_p) will be driven by a concentration gradient[1] This picture of the fracture allows to relate some of the parameters needed

$$n \cdot 2b + 2n \cdot D = a \qquad : D = \frac{a - n \cdot 2b}{2n} \tag{15}$$

$$\epsilon_f = \frac{n \cdot 2b}{a} \qquad : 2b = \epsilon_f (a/n) \tag{16}$$

With this dual–porosity model concept in mind, the following system of differential equations has to be solved for each streamtube [5]:

[1] In the following the word "matrix diffusion" always denotes the diffusion mechanism into the infill material and not into the rock adjacent to the fracture.

$$R_f \frac{\partial C_f^{(k)}}{\partial t} = \frac{\partial}{\partial \eta}\left(a_L \overline{v}_k \frac{\partial C_f^{(k)}}{\partial \eta} - \overline{v}_k C_f^{(k)} \right) + \frac{1}{b} \epsilon_p D_p \left. \frac{\partial C_p^{(k)}}{\partial \xi} \right|_{\xi=b} - \lambda R_f C_f^{(k)} \tag{17a}$$

$$R_p \frac{\partial C_p^{(k)}}{\partial t} = D_p \frac{\partial^2 C_p^{(k)}}{\partial \xi^2} - \lambda R_p C_p^{(k)} \tag{17b}$$

Here, the η–component is aligned with the streamline whereas ξ is the component perpendicular to the (x, y)–plane of the flow field.

The dispersive term $\partial/\partial\eta \ (a_L \overline{v}_k \partial C_f^{(k)}/\partial\eta)$ takes into account that the fractures actually form a network and are multiply connected along the streamlines. The dispersion length a_L is a measure for the distance of such connections.

The following notation has been used

$$R_p = 1 + \frac{(1-\epsilon_p)\rho}{\epsilon_p} K_d \qquad , R_f = 1 + \frac{1}{b} K_a$$

These retention factors assume a linear relation between fluid concentration and adsorbed phase in the fracture as well as in the pore space.

K_a	:	surface related sorption coefficient [m]
K_d	:	volume related sorption coefficient [m^3/kg]
a_L	:	dispersion length [m]
ϵ_p	:	porosity of the infill–matrix [–]
D_p	:	diffusion constant for the infill–matrix [m^2/s]
b	:	half–width of fracture [m]
λ	:	decay constant of tracer substance [s^{-1}]
ρ	:	density of matrix [kg/m^3]
$C_f^{(k)}$	:	tracer concentration [mol/l] in the fracture of width 2b for streamtube k
$C_p^{(k)}$	:	tracer concentration [mol/l] in the matrix pore space for streamtube k

To solve the system of differential equations, eqs. (17a,b) initial and boundary conditions have to be specified:

initial conditions

$$C_p^{(k)}(\xi, t=0) \ = 0 \tag{17c}$$

$$C_f^{(k)}(\eta, t=0) \ = 0 \tag{17d}$$

first boundary conditions

$$\text{in the matrix :} \quad C_p^{(k)}(\xi = b, t) \quad = C_f^{(k)}(\eta, t) \tag{17e}$$

$$\text{in the fracture :} \quad C_f^{(k)}(\eta = 0, t) \quad = f(t) \tag{17f}$$

The function $f(t)$ depends on the way the tracer injection is chosen:

a) step input of duration T_L

$$f(t) = C_{(0)}\left\{\Theta(T_L - t) + e^{-\alpha(t-T_L)}\Theta(t - T_L)\right\} \qquad , \Theta(x) = \begin{cases} 0 & x < 0 \\ 1 & x \geq 1 \end{cases} \tag{17f$_1$}$$

The term $C_{(0)}e^{-\alpha(t-T_L)}\Theta(t-T_L)$ takes into account that the tracer after stopping the injection will start to dilute because of still continuing water injection at a rate Q_i and mixing in the packer volume.

$$\alpha = \frac{Q_i}{V} \qquad , V : \text{volume of packed zone in the injection well} \tag{17f$_2$}$$

In eq. (17f$_1$), T_L is the step duration time and $C_{(0)}$ the concentration of the step input.In all these equations the strong assumption is made that there is an instantaneous and complete mixing within the packed volume.

b) pulse input

$$f(t) = C_{(0)}e^{-\alpha t} \tag{17f$_3$}$$

The meaning of α and $C_{(0)}$ is the same as above

second boundary conditions

$$\text{in the matrix} \quad D_p \left.\frac{\partial C_p^{(k)}}{\partial \xi}\right|_{\xi=D} = 0 \qquad \text{D: maximal penetration depth into matrix} \tag{17g}$$

$$\text{in the fracture} \quad \left.\frac{\partial C_f^{(k)}}{\partial \eta}\right|_{\eta=L_k} = 0 \qquad L_k\text{: length of streamline} \tag{17h}$$

Eq. (17) is solved numerically for all streamtubes with the code RANCHMD [5]. As already mentioned, the final concentration at the collection hole is given by eq. (14).

Some critical comments have to be made to this way of modelling the transport:

-i) It is a bold assumption to model the hydrology as that of an unequal dipole in a homogeneous porous medium of constant width. The medium is neither homogeneous nor of equal thickness; only the attribute "porous" for the fracture infill is probably reasonable.

-ii) The geometry is much simplified: Firstly, the model is a one–dimensional one, secondly the adjacent rock is considered as impermeable (in distinction to usual matrix diffusion models), and thirdly the model completely neglects the influence of the drift.

-iii) The model neglects transversal dispersion completely; however, this is expected to be small since transversal dispersivity is much less than longitudinal dispersivity (at least in the framework of dual porosity models) and gradients between adjacent streamtubes are mostly minor.

-iv) The model assumes constant parameters $(a, b, \overline{v}_k, a_L, K_d, D_p, \epsilon_p)$.
In case of the velocity $\overline{v}_k$ the impact of this assumption can be described qualitatively. That the velocity is not constant can be seen most easily for the streamline $y(x) = 0$ (see eq. (3a)).

$$\mid v \mid\Big|_{y(x)=0} = v_x = \frac{q_x}{\epsilon} = \frac{Q_i}{2\pi a \epsilon}\left(\frac{(\beta+1)l + (\beta-1)x}{l^2 - x^2}\right)$$

This fact is also illustrated in Fig. 6.

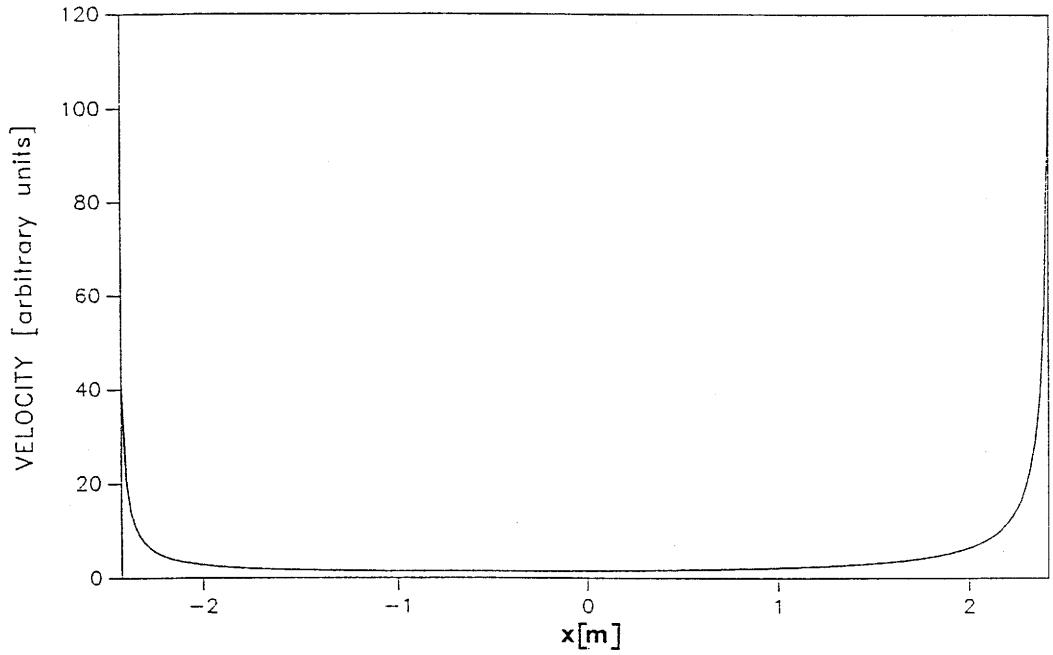

Figure 6: An example of the strongly varying velocity along a streamline. Injection of 77 ml/min at -2.45 m (borehole 4) and 218 ml/min extraction at +2.45 m (borehole 6)

This implies that storage in the matrix perpendicular to the streamline, has not the same magnitude everywhere but is larger in regions where the water velocity is low and smaller at well regions where the velocity is relatively higher[2] (This has to be kept in mind at a stage of possible overcoring and/or excavation).

[2]In this model the average velocity $\overline{v}_0$ along the streamline $y(x) = 0$ (shortest link between boreholes) will be a fit parameter; the velocities of all subsequent streamlines are then given in terms of $\overline{v}_0$: $\overline{v} = \overline{v}_0(L/L_0)/(T/T_0)$ with L, T, T_0 given by eqs. (11), (12) and eq. (13).

4 First results

The model developed in the former sections is confronted with just two experiments performed at Grimsel; the prime aim of this comparison is to see whether a model with so many simplifying assumptions is able to produce any similarity in breakthrough curves with what has been observed in the field.

So far no attempts have been made to extract physical parameters with a best fit procedure [6], as such a procedure would need allocation of very large amounts of computer time: It is eq. (14) that has to be used in this context: If e.g. hundred iterations are needed to find the minimum of the χ^2–function in parameter space, m x 100 RANCHMD calculations have to be performed for all m streamtubes in total (typically m = 20); one RANCHMD computation can take up to 10 minutes. Therefore, to extract physical parameters from a fit procedure to one experiment could need up to 14 days. Therefore, when speaking of a fitted parameter it only means that this particular value can yield a breakthrough curve that roughly matches the experimental data (judgement by eye).

The lack of such a fit procedure is partially compensated in the next section: a parameter variation study may help to build up a qualitative understanding in which range parameters might reproduce experimental findings.

A) Vorversuch 3: nonsorbing uranine

The experiment "Vorversuch 3" has the following characteristics [7]:

a) hydrology: injection at borehole 4 at a rate Q_i = 77 ml/min
withdrawal at borehole 6 at a rate Q_w = 218 ml/min
distance between boreholes : $2l$ = 4.9 m
} β = 2.83

b) tracer pulse input: 40 μgr Uranine (= 1.1 x 10^{-7} mol) into a an effective volume of (packed volume V = 2.1 l. Assuming instantaneous and complete mixing yields
$C_{(0)}$ = 4.9 x 10^{-8} mol/l
The tracer dilution factor α (eq. (17f$_2$)) is given by
α = 1.9 x 10^4 yr^{-1}

For the hydrology of the unequal dipole 20 streamtubes have been chosen per y–halfplane with (for the meaning of C see eq. (9b))

$$C_i - C_{i-1} = \frac{\pi}{20} \qquad C_o = 0 \qquad C_{20} = \pi$$

Therefore each streamtube carries 2.5 % of the input flow rate. The characteristic quantities (T_t, L) for the limiting streamlines can be seen in Table 1 (for streamtubes in the $(y > 0)$–halfplane):

C_{lower}	length L/L_o	time T_t/T_o	$\overline{v}/\overline{v}_o$	
0	1	1	1	
$\pi/20$	1.0015	1.0034	0.9981	) streamtube 1
$2\pi/20$	1.0058	1.0139	0.9920	) streamtube 2
$3\pi/20$	1.0132	1.0316	0.9822	,
$4\pi/20$	1.0237	1.0572	0.9683	,
$5\pi/20$	1.0375	1.0914	0.9506	
$6\pi/20$	1.0548	1.1354	0.9290	
$7\pi/20$	1.0760	1.1908	0.9036	
$8\pi/20$	1.1013	1.2597	0.8743	
$9\pi/20$	1.1314	1.3450	0.8412	
$10\pi/20$	1.1645	1.4502	0.8030	
$11\pi/20$	1.2035	1.5817	0.7609	
$12\pi/20$	1.2526	1.7474	0.7168	
$13\pi/20$	1.3107	1.9592	0.6690	
$14\pi/20$	1.3798	2.2357	0.6172	
$15\pi/20$	1.4629	2.6074	0.5611	
$16\pi/20$	1.5646	3.1281	0.5002	
$17\pi/20$	1.6924	3.9039	0.4335	
$18\pi/20$	1.8603	5.1848	0.3588	
$19\pi/20$	2.1023	7.8053	0.2693	) streamtube 19

Table 1: The limiting streamlines and its characteristics for modelling the experiment "Vorversuch 3" with β = 218/77 and $2l = L_o$ = 4.9 m. L, T_t and T_o are given by eqs. (11a), (12a) and (13). $\overline{v}/\overline{v}_o$ is given by $\overline{v}/\overline{v}_o = (L/L_o)/(T_t/T_o)$.

For the transport model the migration distance in each streamtube has been chosen to be the one of the shorter limiting streamline C_{lower}. (For example for the first streamtube the streamline length of the streamline with $C_{lower} = 0$ has been chosen, i.e. $L_o = 2l$.)

The following transport parameters have been used:

channel half width:	$b = 1.49 \text{ x } 10^{-4}\text{m}$	} flow porosity ϵ_f = 30 %
number of channels:	$n = 10$	
width of fracture:	$a = 1 \text{ x}10^{-2}\text{m}$	
maximum penetration depth:	D = 3.51 x 10^{-4} m	(according to eq. (15))
porosity of the matrix:	ϵ_p = 10 %	
bulk density of matrix:	$\rho(1 - \epsilon_p)$ = 2670 kg/m^3	
sorption coefficients:	$K_a = K_d = 0$	

In Fig. 7 a calculation is shown, where matrix diffusion into fracture infill is turned off, i.e. $D_p = 0$. Then the only parameters to play with were the longitudinal dispersion length a_L and the velocity $\overline{v}_o$.

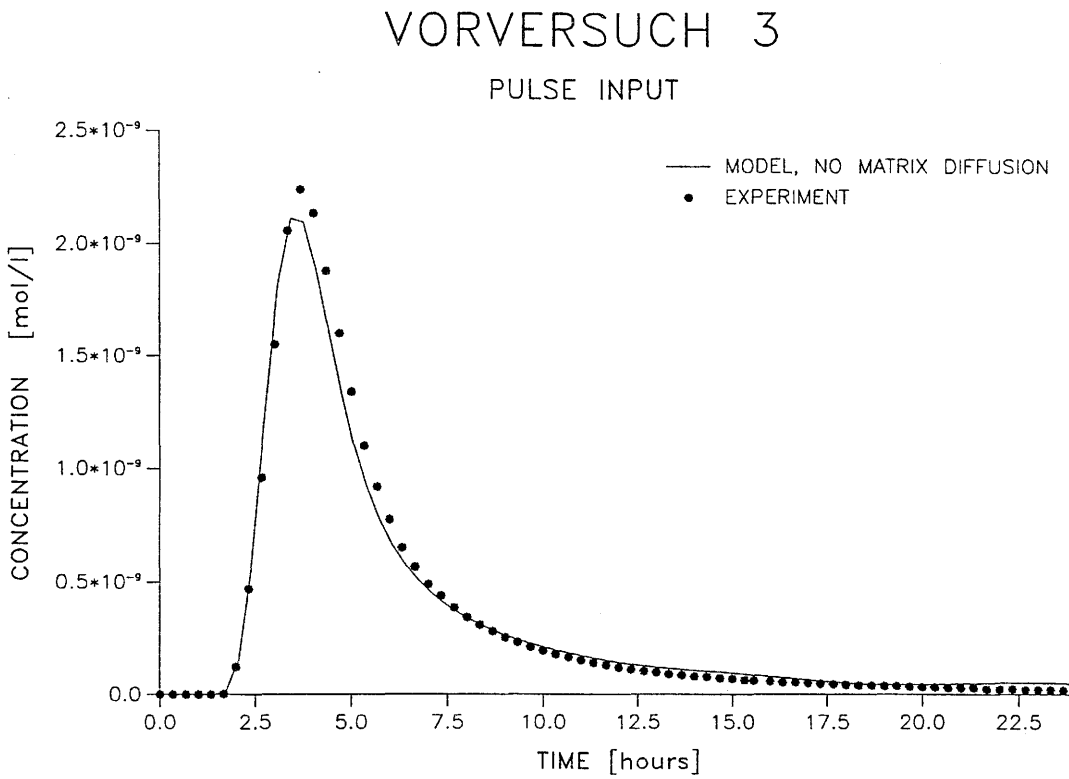

Figure 7: Experimental data of Vorversuch 3 [7] compared with model results from a model assuming no matrix diffusion at all. The parameters chosen are: $\overline{v}_o$ = 14308 m/yr and a_L = 0.10 m. The velocity $\overline{v}_o$ is within the range expected from the hydraulic model [2]. Only selected data point are shown; experimental uncertainties (e.g. mixing in pipes) are unknown.

In Figure 8 matrix diffusion has been turned on. The parameters not yet fixed are given in the caption.

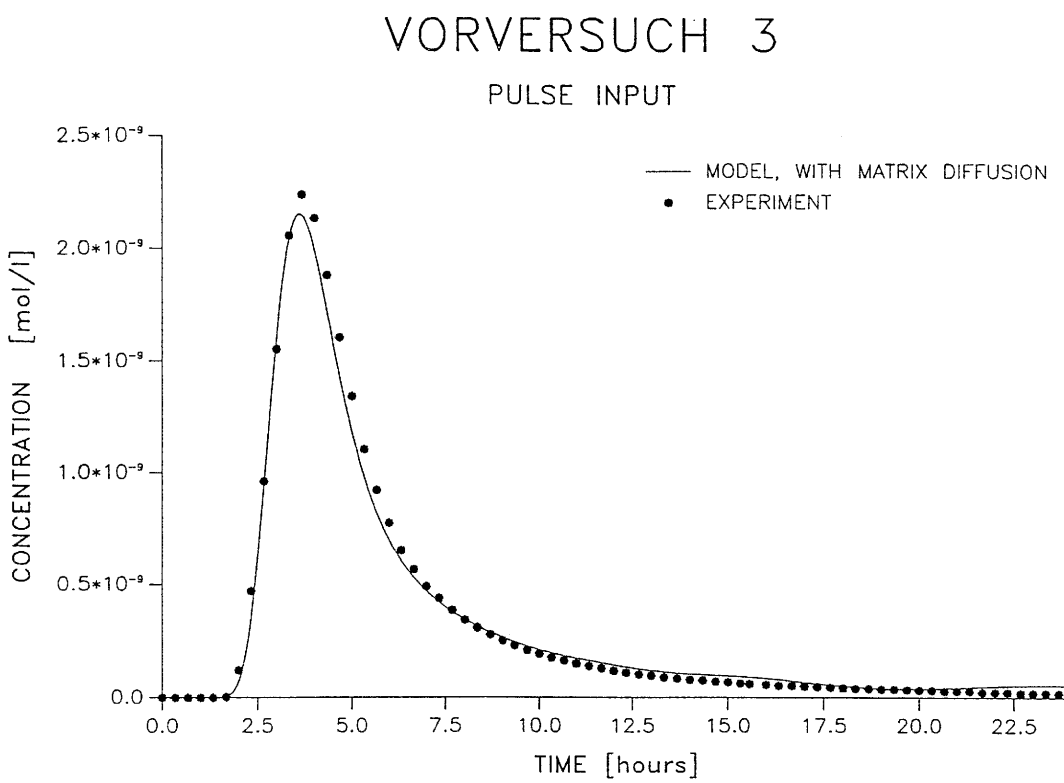

Figure 8: Results with a matrix diffusion model compared with the experimental results of Vorversuch 3 [7]. The parameters used are: $\overline{v}_o$ = 17500 m/yr, a_L = 0.08 m, ϵ_p = 10 %; $\epsilon_p D_p$ = 5 x 10^{-11} m^2/sec.

Comparing these two last figures two remarks have to be made:

i) the velocity $\overline{v}_o$ in case of the matrix diffusion model is larger than in the case of the model without matrix diffusion. This can be understood because the matrix implies a retarding effect such that the velocity has to be increased in order to fit the data.

ii) the broadening of the curve in the case of no matrix diffusion is governed by a_L only, whereas in the case of matrix diffusion, the matrix contributes to the broadening. Thus a_L has to be smaller in the case of modelling with matrix diffusion to reproduce the width of the experimental curve. This is seen in this comparison.

B) Vorversuch 29: nonsorbing uranine and slightly sorbing ^{24}Na

"Vorversuch 29" has been looked at more carefully than others because it is the first experiment in which ^{24}Na was added to conservative tracers. This experiment has the following characteristics [8]:

a) hydrology: injection at borehole 4 at a rate Q_i = 78 ml/min
withdrawal at borehole 6 at a rate Q_w= 165 ml/min } β = 2.12
distance between boreholes : $2l$ = 4.9 m

b) tracer pulse input:
- 1 ml 10 ppm uranine into an effective volume of V = 1.1 l. This yields
  $C_{(0)}$ = 2.5 x 10^{-8} mol/l for uranine
- 4108000 Bq ^{24}Na (= 5.30 x 10^{-13} mol) into the volume V = 1.5 l yields
  $C_{(0)}$ = 5.05 x 10^{-13} mol/l for ^{24}Na

The tracer dilution factor α (eq. (17f$_2$)) is
$\alpha = (Q_{in}/V) = 3.9 \times 10^4\ yr^{-1}$

As in case of Vorversuch 3 the flowfield will be represented by 40 streamtubes with

$$C_i - C_{i-1} = \pi/20 \quad , \quad C_o = 0 \ , \qquad C_{20} = \pi$$

For β = 165/78 a table analogous to Table 1 can be compiled:

C_{lower}	length L/L_o	time T_t/T_o	$\overline{v}/\overline{v}_o$	
0	1	1	1	
$\pi/20$	1.0019	1.0046	0.9973	) streamtube 1
$2\pi/20$	1.0078	1.0187	0.9893	) streamtube 2
$3\pi/20$	1.0177	1.0428	0.9759	,
$4\pi/20$	1.0319	1.0778	0.9574	,
$5\pi/20$	1.0505	1.1251	0.9337	
$6\pi/20$	1.0741	1.1866	0.9052	
$7\pi/20$	1.1030	1.2651	0.8719	
$8\pi/20$	1.1415	1.3624	0.8379	
$9\pi/20$	1.1799	1.4901	0.7918	
$10\pi/20$	1.2269	1.6488	0.7441	
$11\pi/20$	1.2831	1.8525	0.6926	
$12\pi/20$	1.3540	2.1169	0.6396	
$13\pi/20$	1.4389	2.4667	0.5833	
$14\pi/20$	1.5417	2.9416	0.5241	
$15\pi/20$	1.6678	3.6089	0.4621	
$16\pi/20$	1.8257	4.5923	0.3976	
$17\pi/20$	2.0294	6.1456	0.3302	
$18\pi/20$	2.3056	8.8932	0.2593	
$19\pi/20$	2.7196	15.0125	0.1812	) streamtube 19

Table 2: The limiting streamlines and its characteristics for modelling the experiment "Vorversuch 29" with β = 165/78 and $2l = L_o$ = 4.9 m.

The following parameter set gave the best fit to the uranine as well as to the sodium data:

longitudinal dispersion length a_L: a_L = 0.08 m
velocity for streamline $y(x) = 0$: $\overline{v}_o$ = 17500 m/yr
channel half width: b = 1.49 x 10^{-4} m
number of channels: n = 10
width of fracture: a = 1 x 10^{-2} m
maximum penetration depth: D = 3.51 x 10^{-4} m
porosity of the matrix: ϵ_p = 1 %
bulk density of matrix: $\rho(1-\epsilon_p)$ = 2670 kg/m^3
effective diffusivity: $D_p\epsilon_p$ = 2 x 10^{-12} m^2/s
surface sorption coefficient: K_a = 0
volume sorption coefficient: K_d = 0 for uranine
K_d = 3 x 10^{-4} m^3/kg for sodium

The result for uranine is shown in Fig. 9 and for sodium in Fig. 10.

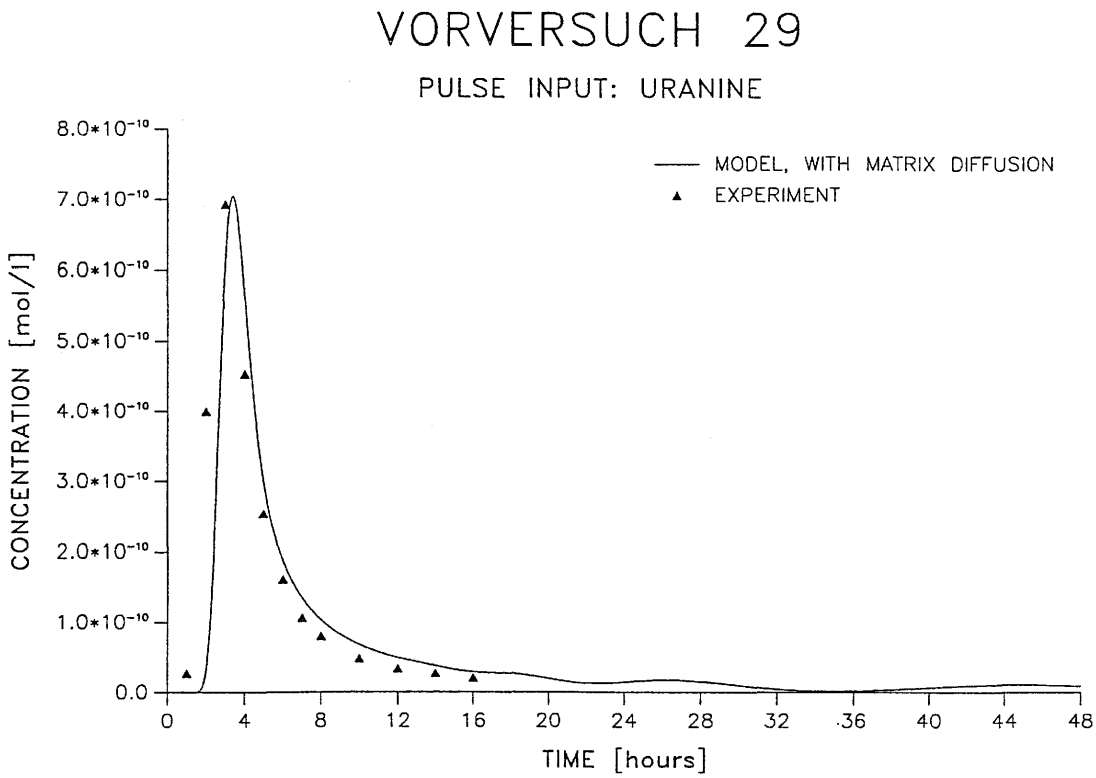

Figure 9: Vorversuch 29: Uranine data versus matrix diffusion model results. The discrepancy at the onset of the breakthrough curve between experiment and model is due to the fact, that the model only tries to fit the peak heights and the tail of the breakthrough curve and completely neglects the slight shoulder the experiment sees at early times.

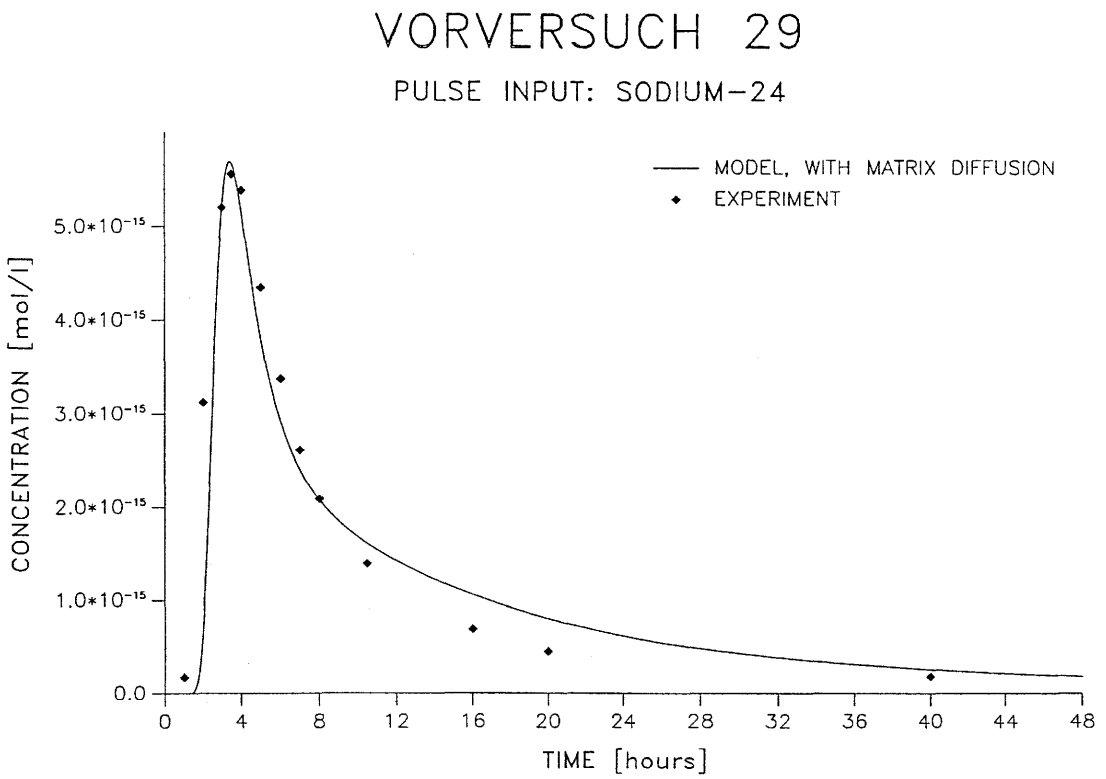

Figure 10: Vorversuch 29: Decay corrected results of a matrix diffusion model compared to experimental data for slightly sorbing ^{24}Na, K_d = 3 x 10^{-4} m^3/kg. See also the caption to Fig. 9.

A remark has to be made about these two figures:

i) In each case, uranine and ^{24}Na, the biggest deviation from observation does not exceed a factor of 2; this of course is not a great achievement but one has to remember three things: Firstly, the model makes very many simplifying assumptions, secondly an optimized fit procedure has not been applied to both of these experiments and thirdly experimental uncertainties are unknown.

5 Parameter variation study

By forgetting the source terms, the equation of motion, eqs. (17a), (17b) can be written in the following form:

$$\begin{aligned} \frac{\partial C_f^{(k)}}{\partial t} &= \alpha_1 \frac{\partial^2 C_f^{(k)}}{\partial \eta^2} + \alpha_2 \frac{\partial C_f^{(k)}}{\partial \eta} + \alpha_3 \frac{\partial C_p^{(k)}}{\partial \xi}\Bigg|_{\xi=b} \\ \frac{\partial C_p^{(k)}}{\partial t} &= \alpha_4 \frac{\partial^2 C_p^{(k)}}{\partial \xi} \end{aligned} \tag{18}$$

where

$$\alpha_1 = \frac{a_L \overline{v}_k}{R_f}$$

$$\alpha_2 = \frac{\overline{v}_k}{R_f}$$

$$\alpha_3 = \frac{1}{b}\frac{\epsilon_p D_p}{R_f}$$

$$\alpha_4 = \frac{D_p}{R_p}$$

Hence, the general solution of eq. (18) in a finite region is characterised by the four parameters $\alpha_1, ..., \alpha_4$. These four "mathematical" parameters are combinations of eight physical parameters $(a_L, \overline{v}_k, b, K_a, \epsilon_p, D_p, \rho, K_d)$. Thus, to extract physical parameters from a fit procedure to experimental data in a unique fashion, four physical parameters have to be taken from independent experiments (or models). The following parameters could be determined in separate experiments:

1. The matrix porosity [9]: ϵ_p = 1 x 10^{-2}
2. The bulk density [9]: $\rho(1-\epsilon_p)$ = 2.67 x 10^3 kg/m^3

For the parameter $\overline{v}_0$ an ad hoc value has been chosen:

3. Flow velocity of shortest path $\overline{v}_0$ = 17000 m/yr

The fracture model, as described in section 3, suggests, that there is no surface sorption in the microfractures (of opening 2b); all the available fracture surfaces are built up by a spongy matrix where diffusion can take place. Thus,

4. Fracture surface sorption coefficient: K_a = 0 m

With the parameters $(\epsilon_p, \rho(1-\epsilon_p), \overline{v}_0, K_a)$ being fixed, a parameter variation study concentrates on the parameter set (a_L, D_p, b, K_d). Since b is defined in terms of the overall–width a, the flow porosity ϵ_f and the number of fractures n, the parameter n will be varied instead, a and ϵ_f being fixed:

i) overall fracture width: $a = 1 \text{ x } 10^{-2}$ m

ii) flow porosity: $\epsilon_f = 2.98 \text{ x } 10^{-1}$

According to eq. (16), the channel width b is then given by:

$$b = \frac{\epsilon_f a}{2} \frac{1}{n}$$

The maximum penetration depth D, to be specified for the location of the matrix boundary condition, is determined by (a, b, n), eq. (15).

For the whole section, the flow rates are kept constant at Q_i = 53 ml/min, Q_w = 150 ml/min (β = 2.83) with $2l$ = 4.9 m.

A) Pulse tests

In subsection A only pulse tests will be considered (T_L = 1 min, eq. (17f$_1$)).

5.A1) Nonsorbing tracers

In this case only three parameters have to be varied, since $K_d = 0$ by definition. Considering (a_L, D_p, n) = (8 x 10^{-2} m, 2 x 10^{-10} m^2/s, 10)
as the base case, the variation range for (a_L, D_p, n) has been chosen to be

$$\begin{aligned} 4 \text{ x } 10^{-2} \text{ m} &\leq a_L \leq 1.2 \text{ x } 10^{-1} \text{ m} \\ 2 \text{ x } 10^{-11} \text{ m}^2/\text{s} &\leq D_p \leq 2 \text{ x } 10^{-9} \text{ m}^2/\text{s} \\ 1 &\leq n \leq 50 \end{aligned}$$

Out of each parameter range only three representatives will be selected

a_L:	$a_1 = 4.0 \text{ x } 10^{-2}$ m	$a_2 = 8.0 \text{ x } 10^{-2}$ m	$a_3 = 1.2 \text{ x } 10^{-1}$ m
D_p:	$D_1 = 2 \text{ x } 10^{-11}$ m^2/s	$D_2 = 2 \text{ x } 10^{-10}$ m^2/s	$D_3 = 2 \text{ x } 10^{-9}$ m^2/s
n:	$n_1 = 1$	$n_2 = 10$	$n_3 = 50$

The variation of n implies the following variation for the opening b of the microfractures and the penetration depth D:

$$\begin{array}{lcll} n = n_1 & : & b = 1.49 \text{ x } 10^{-3} m & , \quad D = 3.51 \text{ x } 10^{-3} m \\ n = n_2 & : & b = 1.49 \text{ x } 10^{-4} m & , \quad D = 3.51 \text{ x } 10^{-4} m \quad \text{(base case)} \\ n = n_3 & : & b = 2.98 \text{ x } 10^{-5} m & , \quad D = 7.02 \text{ x } 10^{-5} m \end{array} \tag{19}$$

The notation (a_i, D_j, n_k) is introduced for the variation where a_L takes on the value a_i, D_p the value D_j and n the value n_k; if any parameter takes on the base case value, a horizontal bar is used. Mathematically, the variations of Table 3 have to be considered:

category A 0 parameter varied	category B 1 parameter varied	category C 2 parameters varied	category D 3 parameter varied
A: (–,–,–)	B1: (a_1,–,–)	C1: (–,D_1,n_1)	D1: (a_1,D_1,n_1)
	B2: (a_3,–,–)	C2: (–,D_1,n_3)	D2: (a_1,D_1,n_3)
	B3: (–,D_1,–)	C3: (–,D_3,n_1)	D3: (a_1,D_3,n_1)
	B4: (–,D_3,–)	C4: (–,D_3,n_3)	D4: (a_1,D_3,n_3)
	B5: (–,–,n_1)	C5: (a_1,–,n_1)	D5: (a_3,D_1,n_1)
	B6: (–,–,n_3)	C6: (a_1,–,n_3)	D6: (a_3,D_1,n_3)
		C7: (a_3,–,n_1)	D7: (a_3,D_3,n_1)
		C8: (a_3,–,n_3)	D8: (a_3,D_3,n_3)
		C9: (a_1,D_1,–)	
		C10: (a_1,D_3,–)	
		C11: (a_3,D_1,–)	
		C12: (a_3,D_3,–)	

Table 3: Possible variations for conservative tracers. Underlined variations have actually been performed.

Varying n and D does not change the shape of the curve.The variation of a_L (Fig 11) shows the well–known property, namely that for a larger (smaller) value of a_L the breakthrough curve gets wider (thinner) with smaller (bigger) peak heights.

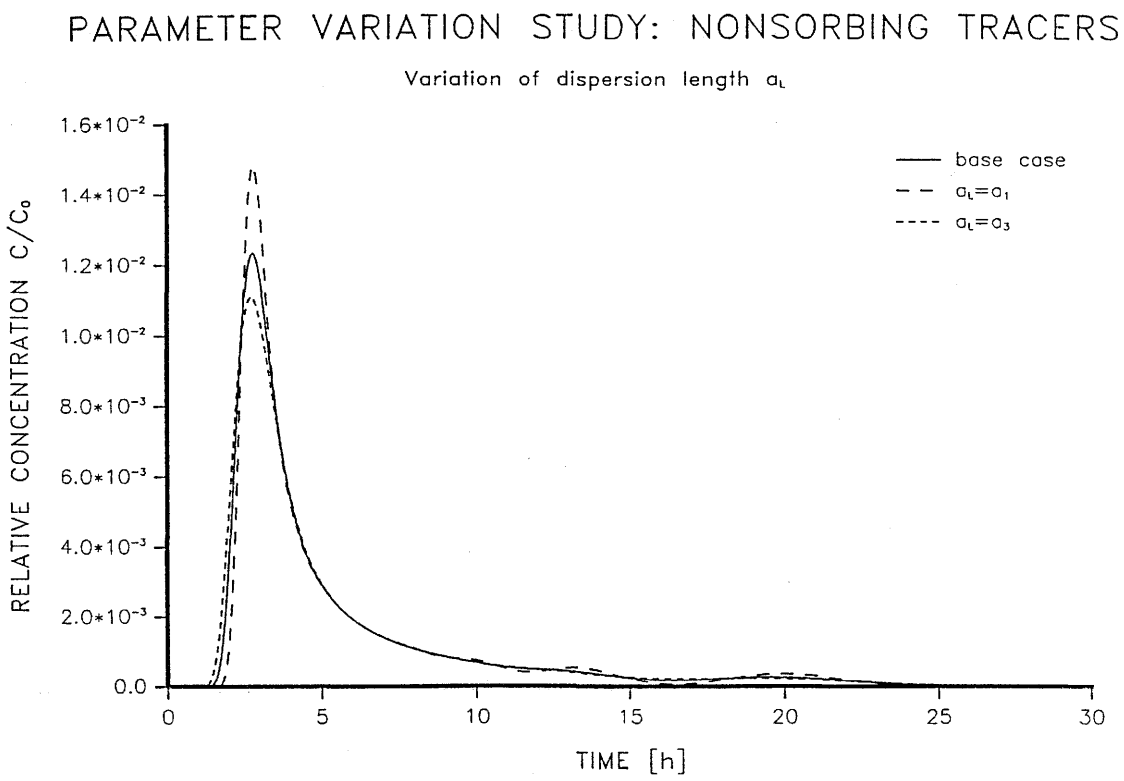

Figure 11: Effect of the variation of a_L on the shape of breakthrough curves. The oscillatory behaviour of the tail is a consequence of poor discretization of long streamlines; this has been tested carefully for the base case but for economical reasons the variations were not redone with a higher resolution.

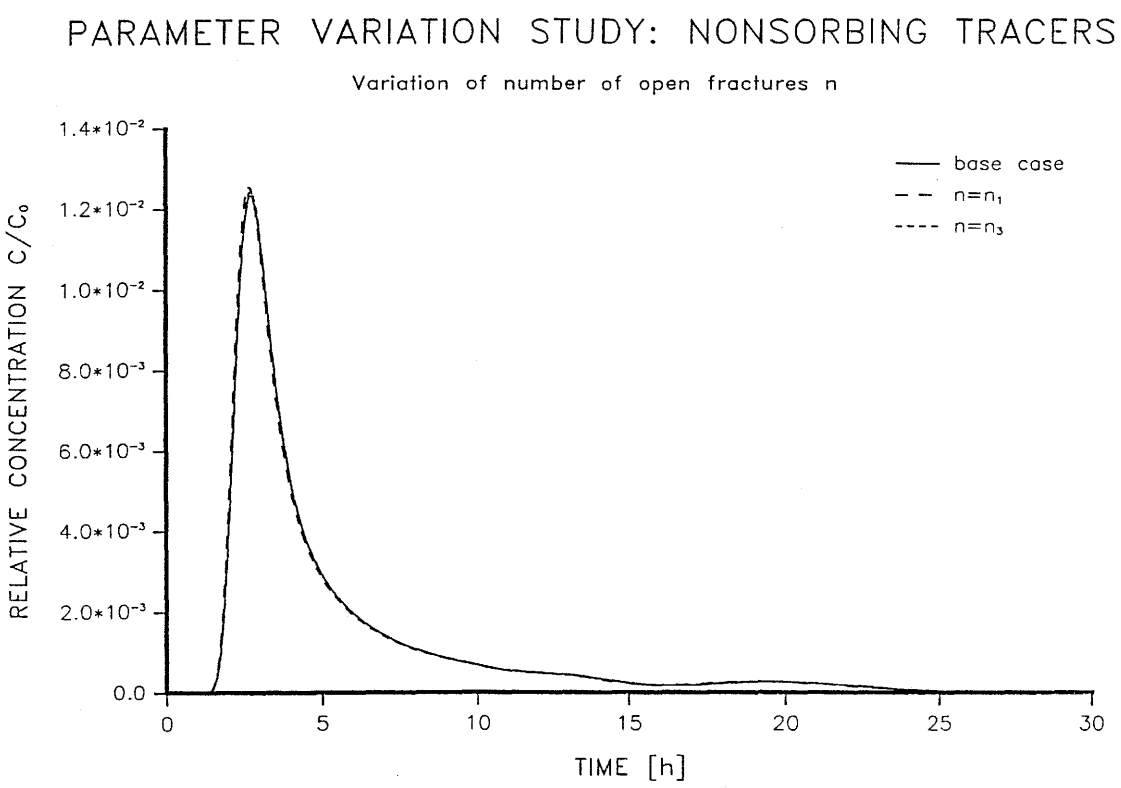

Figures 11b: Effect of n–variations

The very weak dependence of breakthrough curves on (D_p, n) can be understood through the mechanism of fast saturation of the matrix:
The penetration depth $\Delta\xi$ is proportional to $\sqrt{D_p \Delta t}$, where Δt is some characteristic time of the breakthrough curve; for definiteness Δt is the time when the raising part of the breakthrough curve reaches half the peak heights, $\Delta t \simeq 2$h. Thus[3]

$$\Delta\xi_1 = \sqrt{D_1 \Delta t} = 3.79 \text{ x } 10^{-4} \text{ m}$$
$$\Delta\xi_2 = \sqrt{D_2 \Delta t} = 1.20 \text{ x } 10^{-3} \text{ m}$$
$$\Delta\xi_3 = \sqrt{D_3 \Delta t} = 3.79 \text{ x } 10^{-3} \text{ m}$$

For most of the variations considered, the penetration depth $\Delta\xi$ is bigger than the maximum penetration depth D (eq. (19)):

case A:	$\Delta\xi_2$	$>$	3.51 x 10^{-4} m	
case B3:	$\Delta\xi_1$	$\sim$	3.51 x 10^{-4} m	
case B4:	$\Delta\xi_3$	$>$	3.51 x 10^{-3} m	
case B5:	$\Delta\xi_2$	$<$	3.51 x 10^{-3} m	and thus a slight deviation from the base case
case B6:	$\Delta\xi_2$	$>$	7.02 x 10^{-5} m	

Thus matrix saturation occurs; as a consequence, the shape of the breakthrough curves is no longer sensitive to matrix properties (D_p) or its geometry (n, i.e. b and D).

The results of category C (two–parameter variations) are shown in the Figs. 12a,b,c.

[3]The consant of proportionality has been put equal to 1. This is strictly true only for an infinite medium; however, this value is an upper bound for the penetration depth within a finite medium.

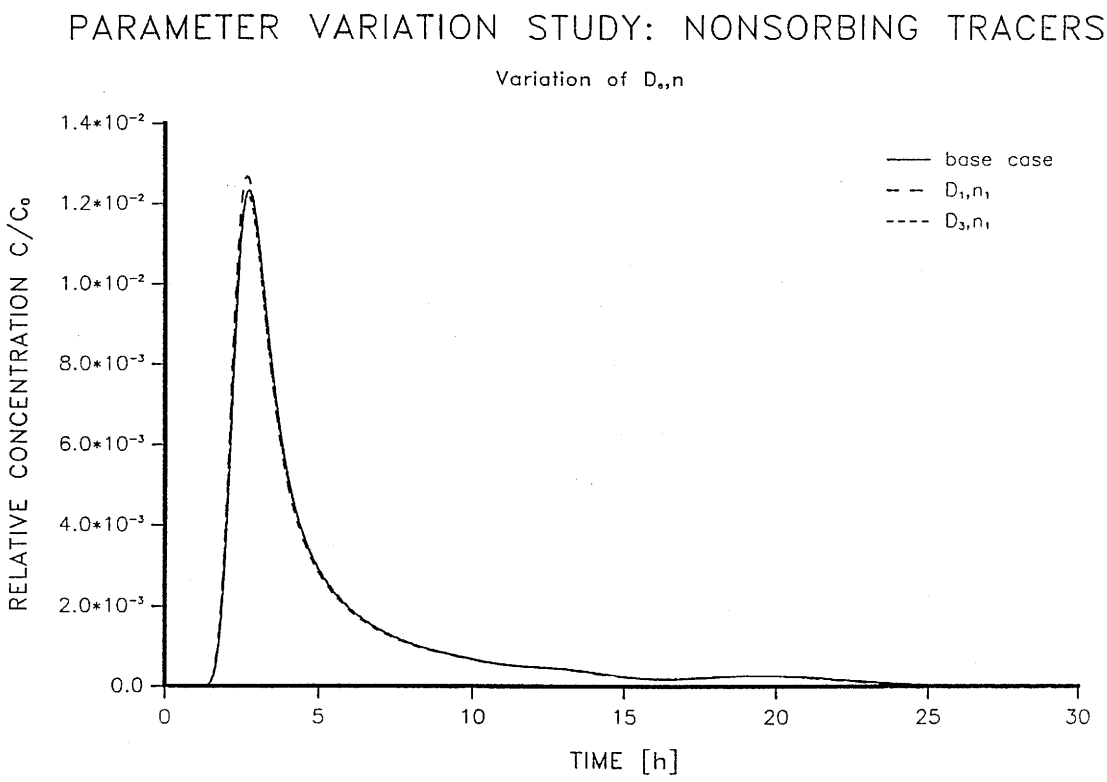

Figures 12 a: Effects of (–,D_i, n_j)–variations on the shape of breakthrough curves.

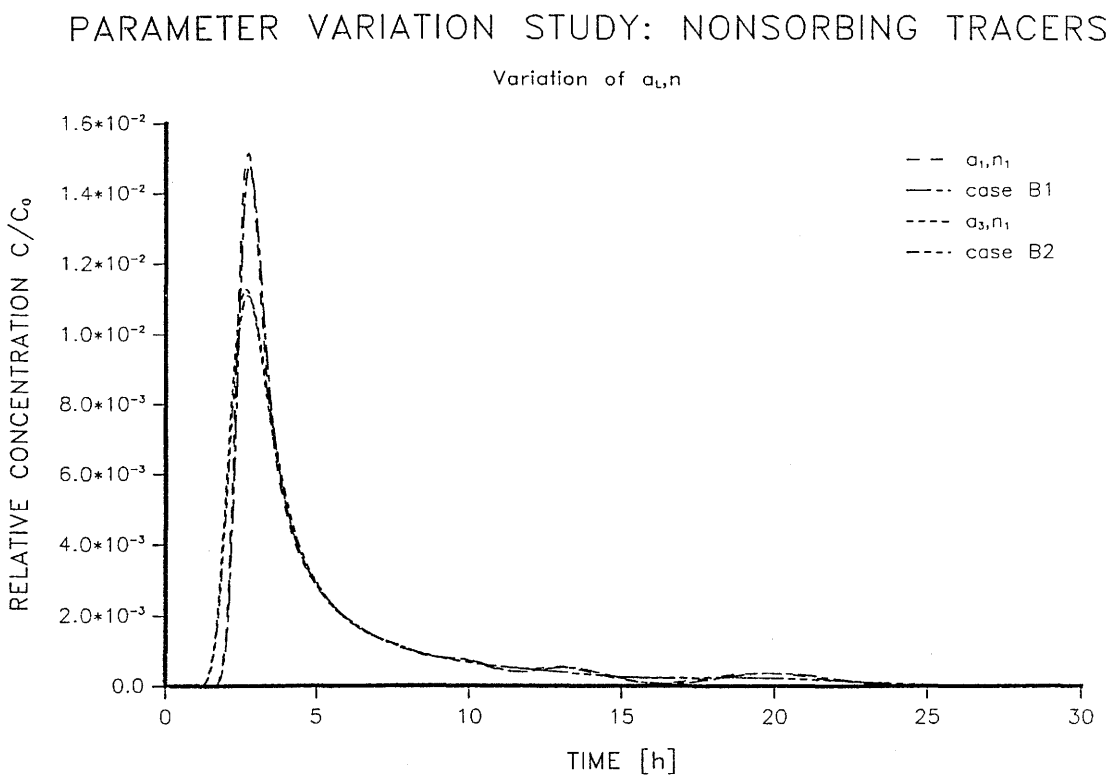

Figures 12 b: Effects of $(a_i,-,n_j)$–variations on the shape of breakthrough curves.

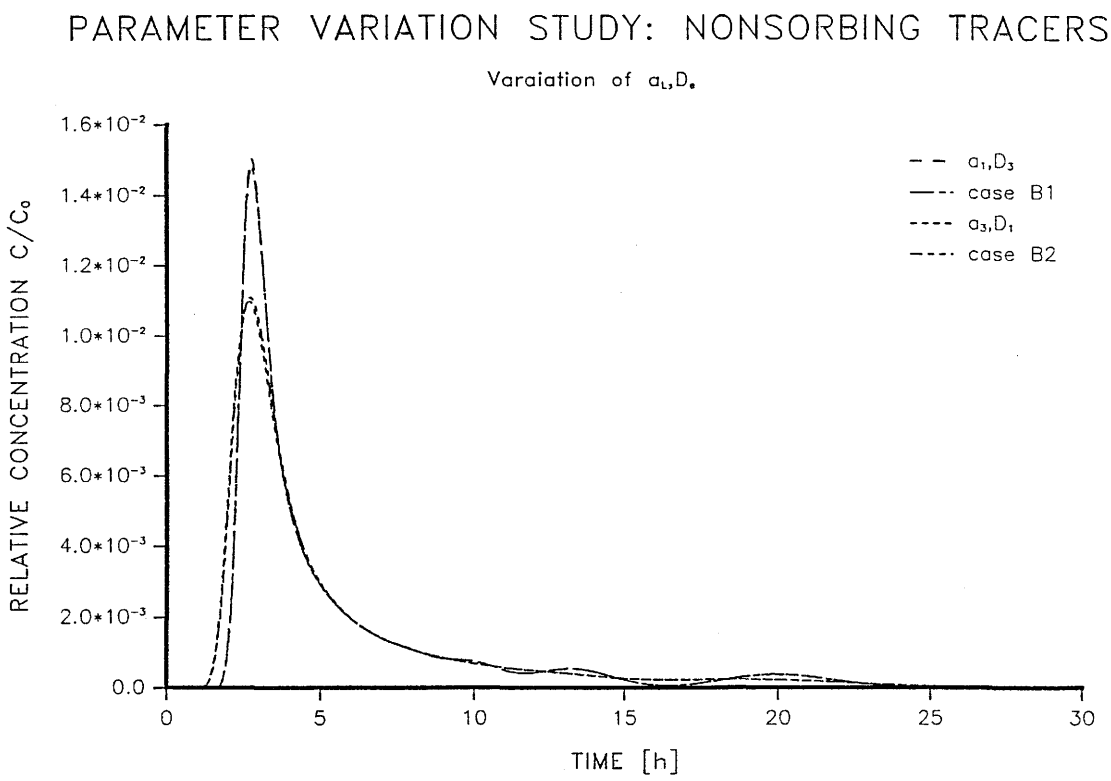

Figures 12 c: Effects of $(a_i, D_j, –)$–variations on the shape of breakthrough curves.

Not all the possible variations of category C have been calculated because the few calculated cases already show that the behaviour of these variations is completely determined by quick and complete matrix saturation, too; all the arguments mentioned above about penetration depth versus matrix width apply here as well. The cases $(a_1, D_j, n_k), (a_3, D_j, n_k)$ closely follow the one–parameter variations $(a_1, –, –)$ (case B1) and $(a_3, –, –)$ (case B2), as it should be if the saturation argument has to hold.

Only one variation of category D has been calculated, (a_3, D_1, n_1). The result is shown in Figure 13. Again, its behaviour can fully be understood in terms of fast matrix saturation.

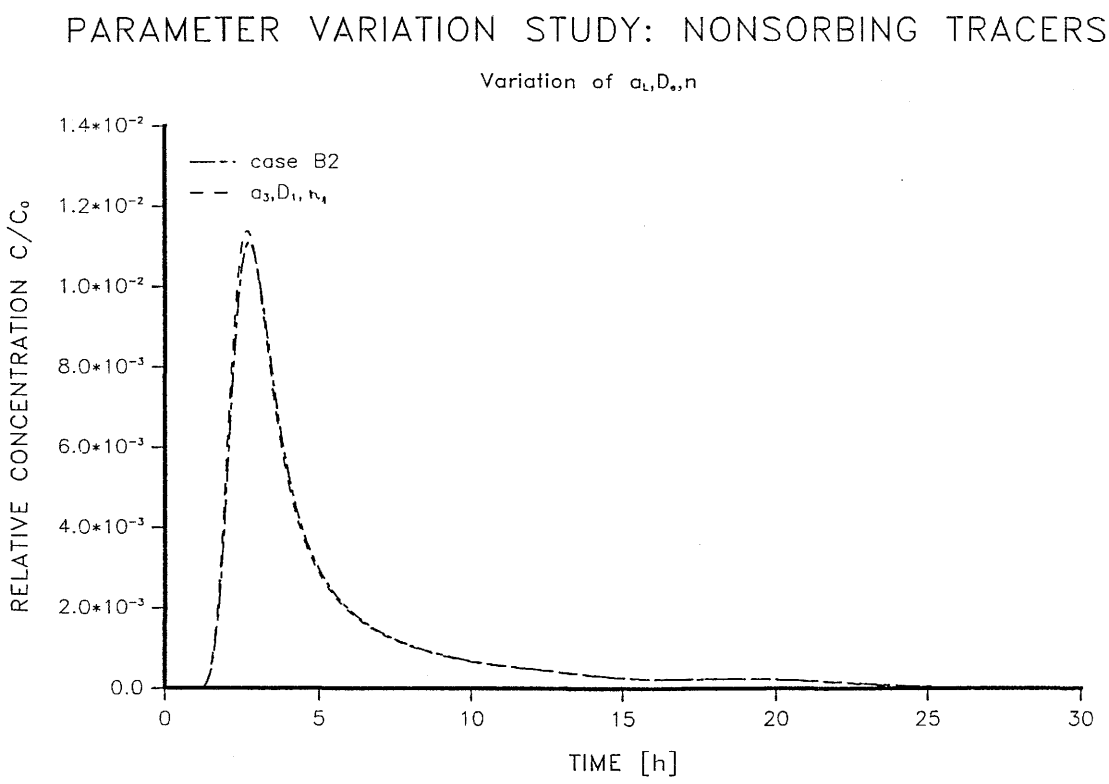

Figure 13: Impact of a three–parameters variation on the shape of a breakthrough curve.

5.A2) Sorbing tracers

For sorbing tracers, the general case, where 4 parameters may be varied, has to be studied.

The parameter set
(a_L, D_p, n, K_d) = (8 x 10^{-2} m, 2 x 10^{-10} m^2/s, 10, 3 x 10^{-4} m^3/kg)
defines the base case, whereas

a_L:	a_1 = 4 x 10^{-2} m	a_2 = 8 x 10^{-2} m	a_3 = 1.2 x 10^{-1} m
D_p:	D_1 = 2 x 10^{-11} m^2/s	D_2 = 2 x 10^{-10} m^2/s	D_3 = 2 x 10^{-9} m^2/s
n:	n_1 = 1	n_2 = 10	n_3 = 50
K_d:	K_1 = 3 x 10^{-5} m^3/kg	K_2 = 3 x 10^{-4} m^3/kg	K_1 = 3 x 10^{-3} m^3/kg

sets the values for all possible variations listed in Table 4.

category E 0 parameter varied	category F 1 parameter varied	category G 2 parameters varied	category H 3 parameter varied	category I 4 parameters varied
E: (–,–,–,–)	F1: (a_1,–,–,–)	G:1: (a_1, D_1,–,–)	H1: (a_1, D_1, n_1,–)	I1: (a_1, D_1, n_1, K_1)
	F2: (a_3,–,–,–)	G2: (a_1, D_3,–,–)	H2: (a_1, D_1, n_3,–)	I2: (a_1, D_1, n_1, K_3)
	F3: (–,D_1,–,–)	G3: (a_3, D_1,–,–)	H3: (a_1, D_3, n_1,–)	I3: (a_1, D_1, n_3, K_1)
	F4: (–,D_3,–,–)	G4: (a_3, D_3,–,–)	H4: (a_1, D_3, n_3,–)	I4: (a_1, D_1, n_3, K_3)
	F5: (–,–,n_1,–)	G5: (a_1,–,n_1,–)	H5: (a_3, D_1, n_1,–)	I5: (a_1, D_3, n_1, K_1)
	F6: (–,–,n_3,–)	G6: (a_1,–,n_3,–)	H6: (a_3, D_1, n_3,–)	I6: (a_1, D_3, n_1, K_3)
	F7: (–,–,–,K_1)	G7: (a_3,–,n_1,–)	H7: (a_3, D_3, n_1,–)	I7: (a_1, D_3, n_3, K_1)
	F8: (–,–,–,K_3)	G8: (a_3,–,n_3,–)	H8: (a_3, D_3, n_3,–)	I8: (a_1, D_3, n_3, K_3)
		G9: (a_1,–,–,K_1)	H9: (a_1, D_1,–,K_1)	I9: (a_3, D_1, n_1, K_1)
		G10: (a_1,–,–,K_3)	H10: (a_1, D_1,–,K_3)	I10: (a_3, D_1, n_1, K_3)
		G11: (a_3,–,–,K_1)	H11: (a_1, D_3,–,K_1)	I11: (a_3, D_1, n_3, K_1)
		G12: (a_3,–,–,K_3)	H12: (a_1, D_3,–,K_3)	I12: (a_3, D_1, n_3, K_3)
		G13: (–,D_1, n_1,–)	H13: (a_3, D_1,–,K_1)	I13: (a_3, D_3, n_1, K_1)
		G14: (–,D_1, n_3,–)	H14: (a_3, D_1,–,K_3)	I14: (a_3, D_3, n_1, K_3)
		G15: (–,D_3, n_1,–)	H15: (a_3, D_3,–,K_1)	I15: (a_3, D_3, n_3, K_1)
		G16: (–,D_3, n_3,–)	H16: (a_3, D_3,–,K_3)	I16: (a_3, D_3, n_3, K_3)
		G17: (–,D_1,–,K_1)	H17: (a_1,–,n_1, K_1)	
		G18: (–,D_1,–,K_3)	H18: (a_1,–,n_1, K_3)	
		G19: (–,D_3,–,K_1)	H19: (a_1,–,n_3, K_1)	
		G20: (–,D_3,–,K_3)	H20: (a_1,–,n_3, K_3)	
		G21: (–,–,n_1, K_1)	H21: (a_3,–,n_1, K_1)	
		G22: (–,–,n_1, K_3)	H22: (a_3,–,n_1, K_3)	
		G23: (–,–,n_3, K_1)	H23: (a_3,–,n_3, K_1)	
		G24: (–,–,n_3, K_3)	H24: (a_3,–,n_3, K_3)	
			H25:(–,D_1, n_1, K_1)	
			H26:(–,D_1, n_1, K_3)	
			H27:(–,D_1, n_3, K_1)	
			H28:(–,D_1, n_3, K_3)	
			H29:(–,D_3, n_1, K_1)	
			H30:(–,D_3, n_1, K_3)	
			H31:(–,D_3, n_3, K_1)	
			H32:(–,D_3, n_3, K_3)	

Table 4: Possible variations for sorbing tracers. The notation is a straightforward extension of that one for conservative tracers. Underlined variations have actually been calculated.

The one–parameter variations of category F are shown in Figs. 14a, ...,14d.

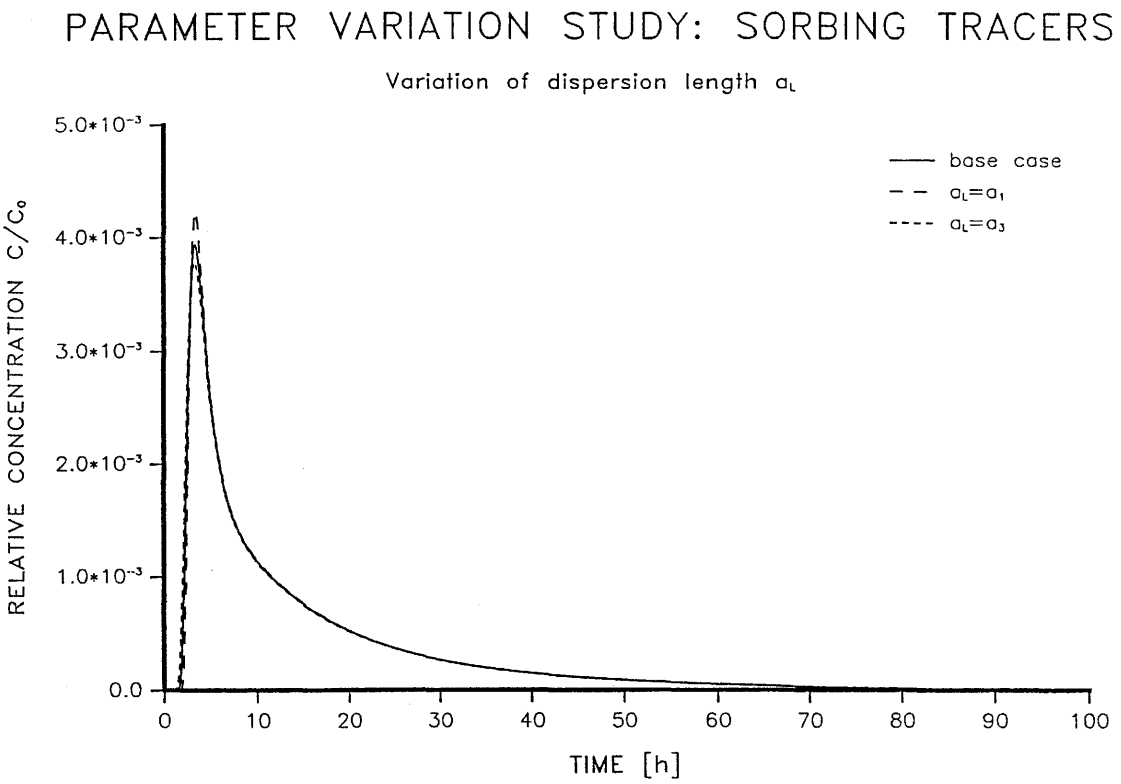

Figure 14a: Variation of the dispersion length a_L

The effect of varying the dispersion length a_L (Fig. 14a) is small and can mainly be seen in the raising part of the breakthrough curve and the peak heights; there is no a_L–sensitivity in the tail of the breakthrough curve due to the fact that all streamtubes contribute to the tail and this results in a smearing of that part (In contrast, the peak location and the peak heights is mainly determined by the shortest flowpaths).

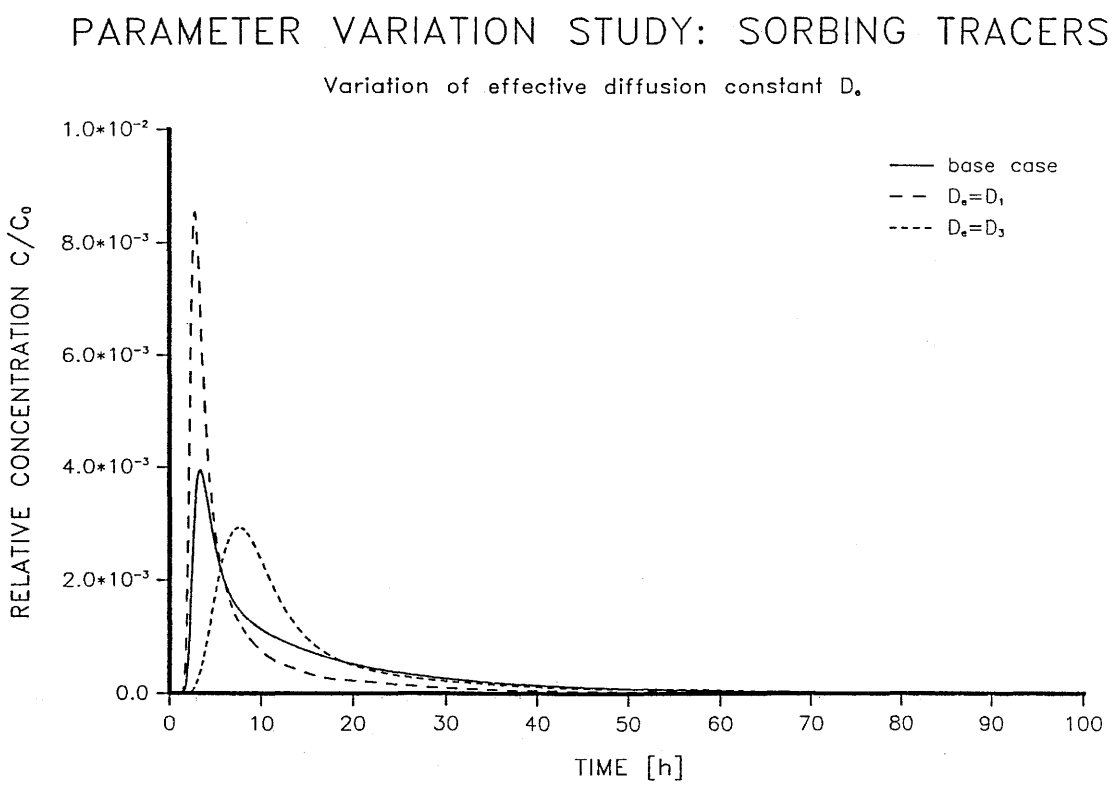

Figure 14b: Variation of $\epsilon_p D_p$

The $\epsilon_p D_p$–variations, as shown in Fig. 14b, show a significant dependency of breakthrough curves on this parameter: lowering the value with respect to the base case leads to a higher and (because of mass conservation) sharper peak because the less permeable matrix acts almost like a dam: only little tracer can penetrate into the matrix resulting in a relatively quick flushing of the tracer through the open fractures. Increasing the $\epsilon_p D_p$–value to 2 x 10^{-11} m^2/s on the other hand allows the tracer to partially penetrate into the matrix; the matrix acts as a storage and releases the mass only over a relatively long period of time; therefore the peak height is lower and the breakthrough curve wider.

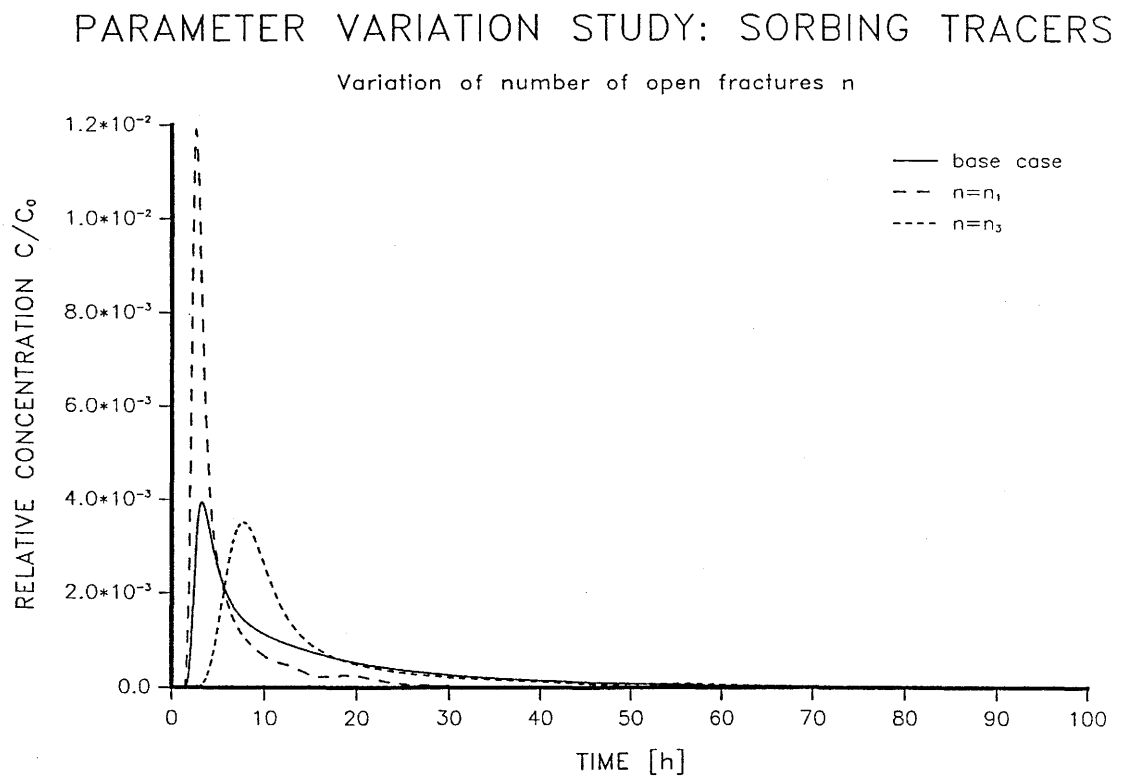

Figure 14c: Variation of n

Varying the number of open fractures (see Fig 14c) leads to a similar pattern as in case of varying $\epsilon_p D_p$. In having only one open fracture ($n = n_1$) the tracer sees only little matrix surface where to intrude and thus gets flushed through quickly. If there are many open fractures (e.g. $n = n_3 = 50$) the directly accessible matrix volume is much larger and thus storing tracer there is easily possible; this results in retarding and lowering the breakthrough curve quite drastically.

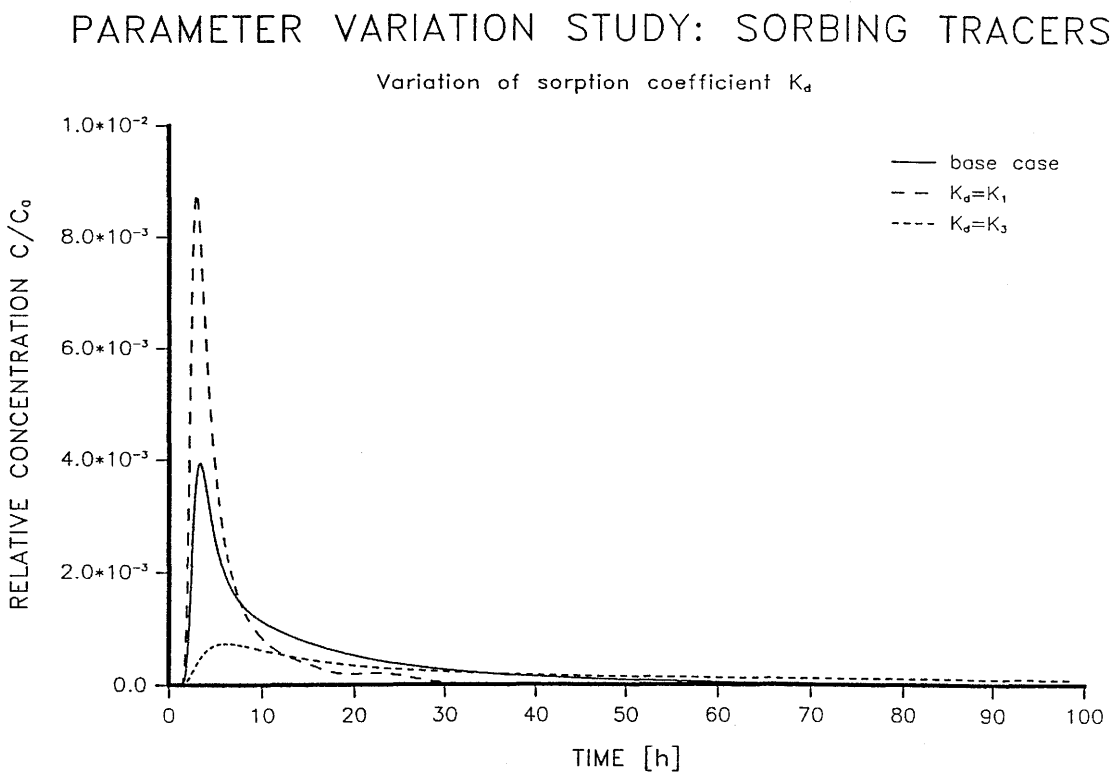

Figure 14d: Variation of the sorption coefficient K_d

The variation of the K_d–value (Fig. 14d) shows the well known effects and thus is not commented any further.

Some variations of category G (2 parameters varied) are illustrated in the Figs. 15a, ...,15d. The reasons for the selection of particular variations are the following:

i) the variations on a_L alone show very little effect on the shape of breakthrough curves and hence, it is expected that the variations (a_L, D_i,–,–,), (a_L,–,n_j,–), (a_L,–,–,K_j) follow the variation pattern of (–,D_i,–,–), (–,–,n_j,–) and (–,–,–,K_j) respectively; thus, random samples were chosen for the variations where a_L was one of the two parameters to be varied. These variations are shown in Fig. 15a.

ii) For variations (–,D_i, n_j,–), (–,–,n_i, K_j), (–,D_i,–,K_j) it can be expected from the outcome of the variations of category F that all three pairs are anticorrelated (at least in case of no saturation of the infill–matrix) and therefore the variations (–,D_1, n_3,–), (–,D_3, n_1,–); (–,D_1,–,K_3), (–,D_3,–,K_1); (–,–,n_1, K_3), (–,–,n_3, K_1) were chosen.

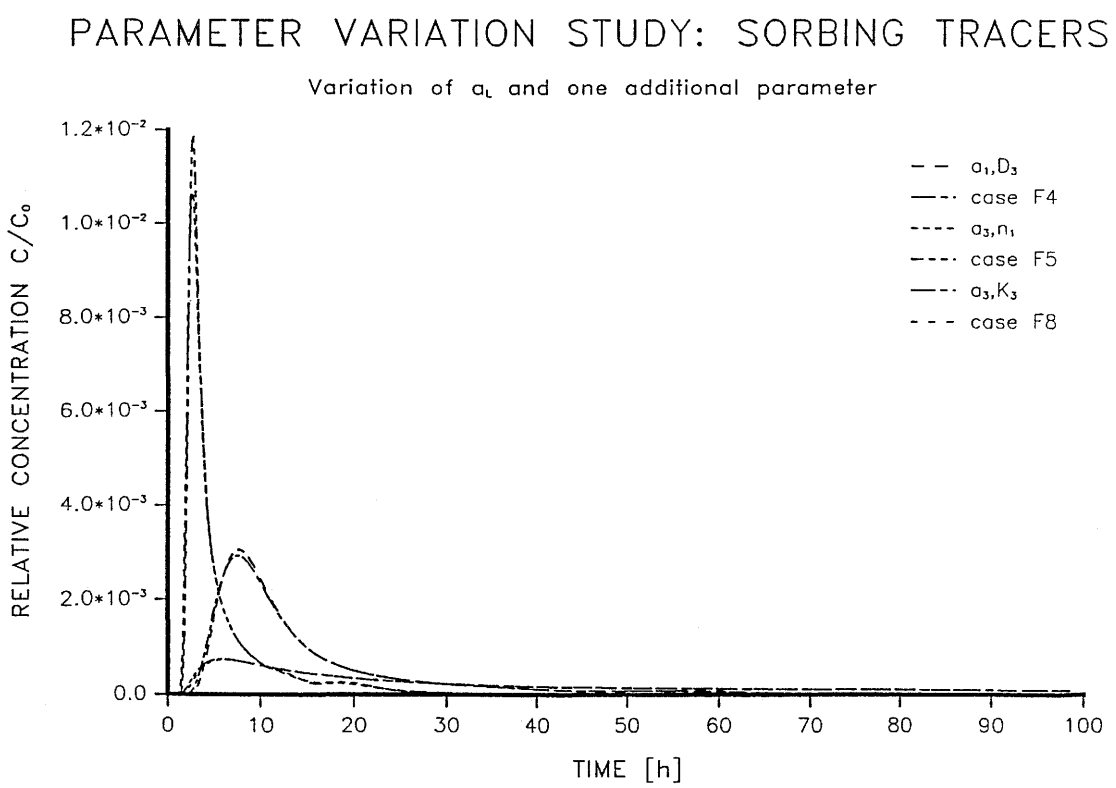

Figure 15a: Variation of a_L and one additional parameter

It can be seen that for all variations of Fig. 15a the shape of the breakthrough curves is dictated by the variation of either D_e, n or K_d and not by the variation of a_L. This can be understood quite easily: As shown in Fig. 14a, the a_L–dependence is weak, whereas the dependence on D_e, n and K_d is quite strong.

Variations of the form $(-, D_i, n_j, -)$ are shown in Fig. 15b:

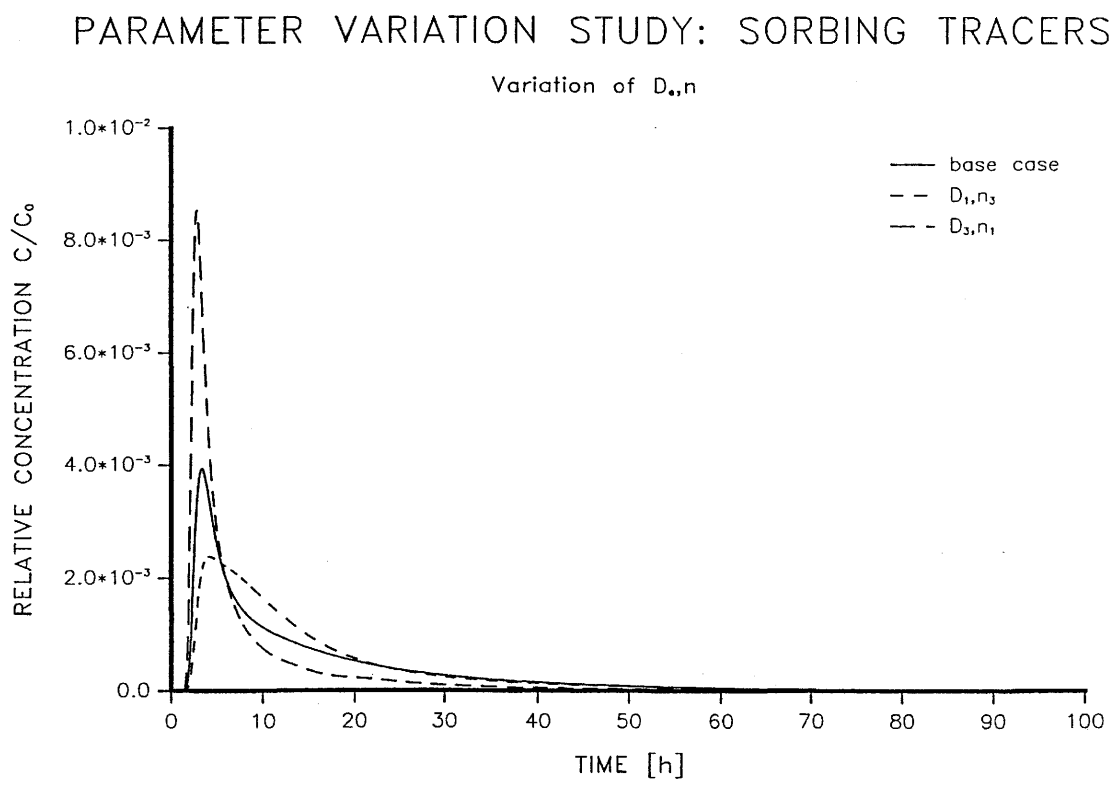

Figure 15b: Variation of the form (–,D_i, n_j,–)

The case (–,D_1, n_3,–) shows that the dam effect of a small diffusion constant determines the first arrival time whereas the matrix sorption capacity for the case n_3 gets apparent at later times only. For the variation (–,D_1, n_3,–) the peak shape and its location is dictated by the single channel. The fact that the tail for (–,D_1, n_3,–) is bigger than for (–,D_3, n_1,–) can be explained by higher partial saturation of the matrix in case of (–,D_1, n_3,–). (The penetration depth $\Delta\xi$ for a sorbing tracer is proportional to $\sqrt{(D_p/R_p)\Delta t}$; see also subsection 5.1).

In Fig. 15c (–,D_i, K_j,–) variations are shown.

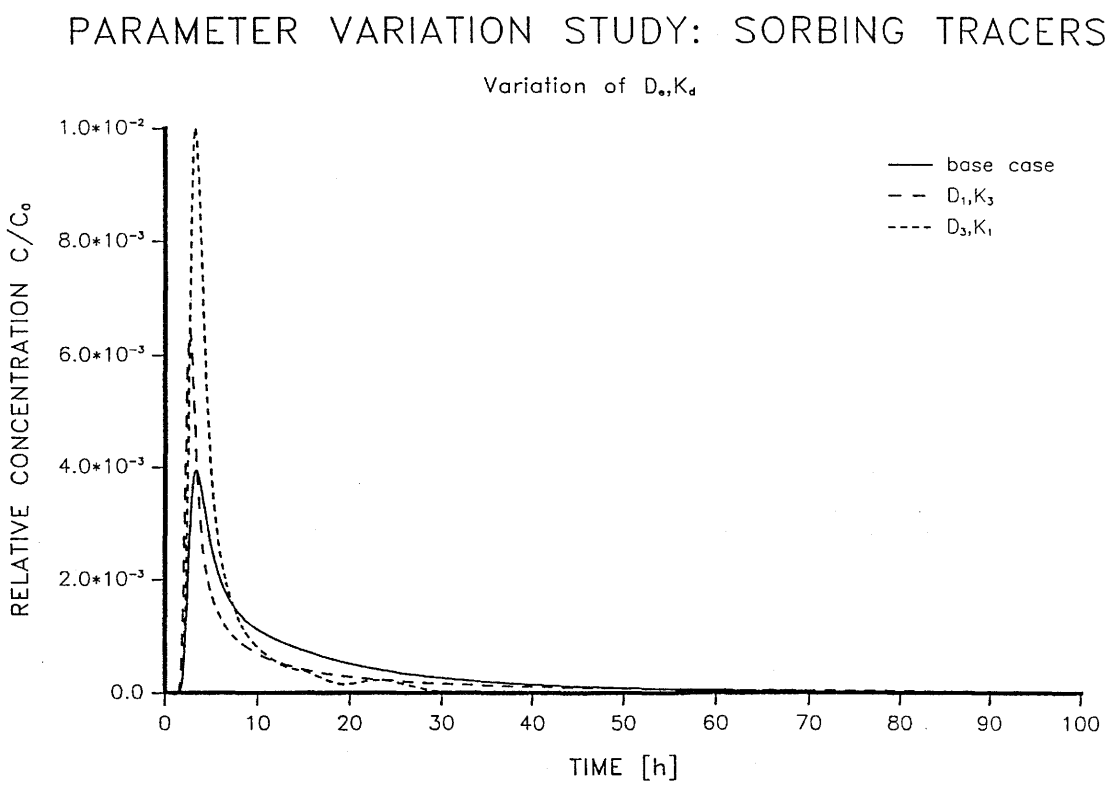

Figure 15c: Variation of the form (–,D_i, K_j,–)

The variation (–,D_1, K_3,–) has the peak at the same time as the case (–,D_1,–,–) but at a reduced height due to a strong sorption tendency in the matrix. The case (–,D_3, K_1,–) shows a behaviour that, at first is quite surprising: the peak height is higher than for the case (–,–,–,K_1). Because the matrix is quite permeable and the sorption only weak, saturation of the matrix happens in less than two hours and thus the same characteristics as in case of nonsorbing tracers can be seen: pretty fast exchange of material between the fracture and the matrix and thus also a very strongly peaked breakthrough; in the case of (–,–,–K_1) no saturation is happening within 2 hours time.

The last variation performed for category G is shown in fig. 15d.

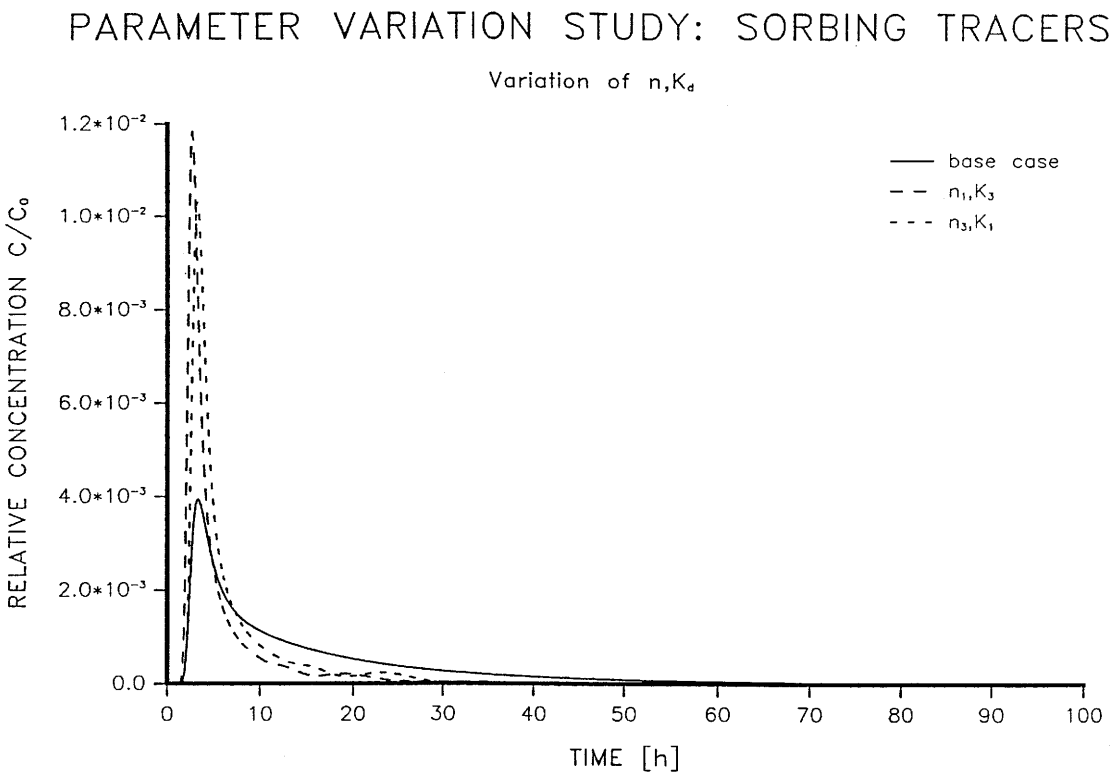

Figure 15d: Variation of the form $(-,-,n_i,K_j)$

The variation $(-,-,n_1,K_3)$ is indistinguishable from the variation $(-,-,n_1,-)$; this can be explained by the very small penetration of tracer into the matrix: For K_3 : $\Delta\xi(K_3)$ = 4.3 x 10^{-5} m $\ll$ 3.51 x 10^{-3} m and for K_2 : $\Delta\xi(K_2)$ = 1.3 x 10^{-4} m $\ll$ 3.51 x 10^{-3} m. Therefore fast transport through the fracture dominates these variations. In case of variation $(-,-,n_3,K_1)$ the opposite is true $\Delta\xi(K_1)$ = 4.0 x 10^{-4} m > 7.02 x 10^{-5} m and therefore a fast exchange of mass between fracture and matrix happens; this also leads to a relatively fast and sharply peaked breakthrough, but with a tail that is bigger than in case $(-,-,n_1,K_3)$.

Concerning the variations of category H (variation of 3 parameters) only variations of the form $(-,D_i,n_j,K_k)$ have been studied; due to the gained experience it is expected that the discrepancies between $(a_l,-,n_j,K_k)$, $(a_l,D_i,-,K_k)$ or $(a_l,D_i,n_j,-)$, $l \neq 2$ and $(-,-,n_j,K_k)$, $(-,D_i,-,K_k)$ or $(-,D_i,n_j,-)$ respectively are minor and well understood.

The variations shown in Fig. 16 were selected in order to see the behaviour of breakthrough curves as a function of saturation.

case H27: $\Delta\xi(K_1)$ = 1.27 x 10^{-4} m > $D(n_3)$ = 7.02 x 10^{-5} m
case H28: $\Delta\xi(K_3)$ = 1.35 x 10^{-5} m $\sim \frac{1}{5}D(n_3)$ = 7.02 x 10^{-5} m
case H30: $\Delta\xi(K_3)$ = 1.35 x 10^{-5} m $\ll D(n_1)$ = 3.51 x 10^{-3} m

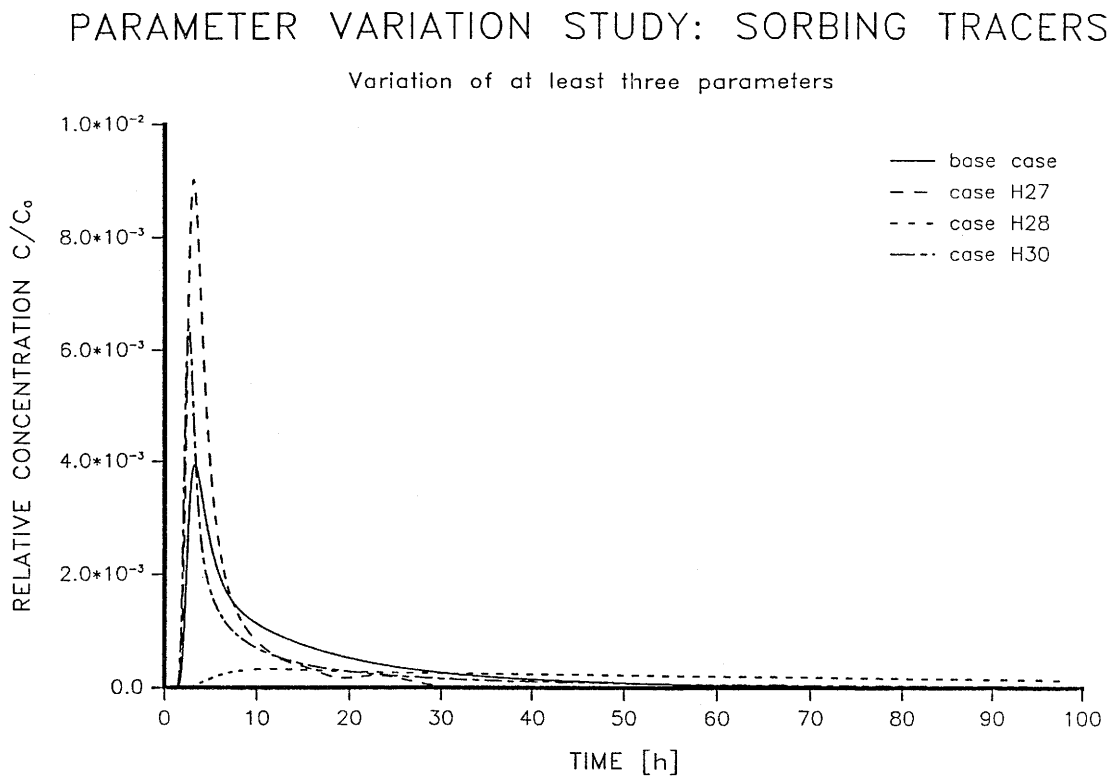

Figure 16: Variation of at least three parameters

The same behaviour, as discussed earlier, can be seen here: If saturation is reached (case H27) the tracer exchange between matrix and fracture is fast and a sharply peaked breakthrough curve is the result. If quite a proportion of tracer has diffused into the infill matrix and sorption is strong (case H28) then the temporal concentration profile is flat and extends to long times. If very little saturation has occurred (case H30) the profile very much resembles the breakthrough curve of a pure fracture model.

No variation of category I was studied because no big effects are expected: The differences between (a_i, D_j, n_k, K_l) and $(-, D_j, n_k, K_l)$ are certainly of the same order as the ones between $(a_i,-,-,-)$ and $(-,-,-,-)$.

B) Step input tests

In the former subsection A only pulse tests were considered and it could be seen that the effect of a variation strongly depended on the degree of saturation of the infill–matrix. To probe the eventual process of matrix diffusion most efficiently the matrix should get saturated completely; this can be achieved with step input tests: After stopping the tracer input the matrix releases the stored tracer over a long period of time and thus the tail of such a breakthrough curve is quite sensitive to the mechanisms of matrix diffusion. It is clear that such a detailed variation study as performed for pulse tests cannot be performed; computer time consumption would be enormous. Therefore only a few calculations will be presented; at that stage (summer 90) they might be of relevance for the experimental program at Grimsel.

The hydraulic arrangement is the same as for the pulse test variation study.

Q_i = 53 ml/min (at borehole 4)
Q_w= 150ml/min (at borehole 6) $\rightarrow \beta = 2.83$ (→ see Table 1)

distance between boreholes: $2l$ = 4.9 m
dilution factor: $\alpha = 1.1 \times 10^5\ yr^{-1}$ (V = 250ml)

The parameters chosen are the ones of the base case; three values have been taken for the K_d–value.

$K_1 = 0$ (e.g. uranine)
$K_2 = 3 \times 10^{-4}\ m^3/kg$ (e.g. Na)
$K_3 = 1.8 \times 10^{-2}\ m^3/kg$ (e.g. Sr)

The step length T_L (eq. ($17f_1$)) is set equal to two weeks (336 hours). The results of this step input variation are shown in Fig. 17.

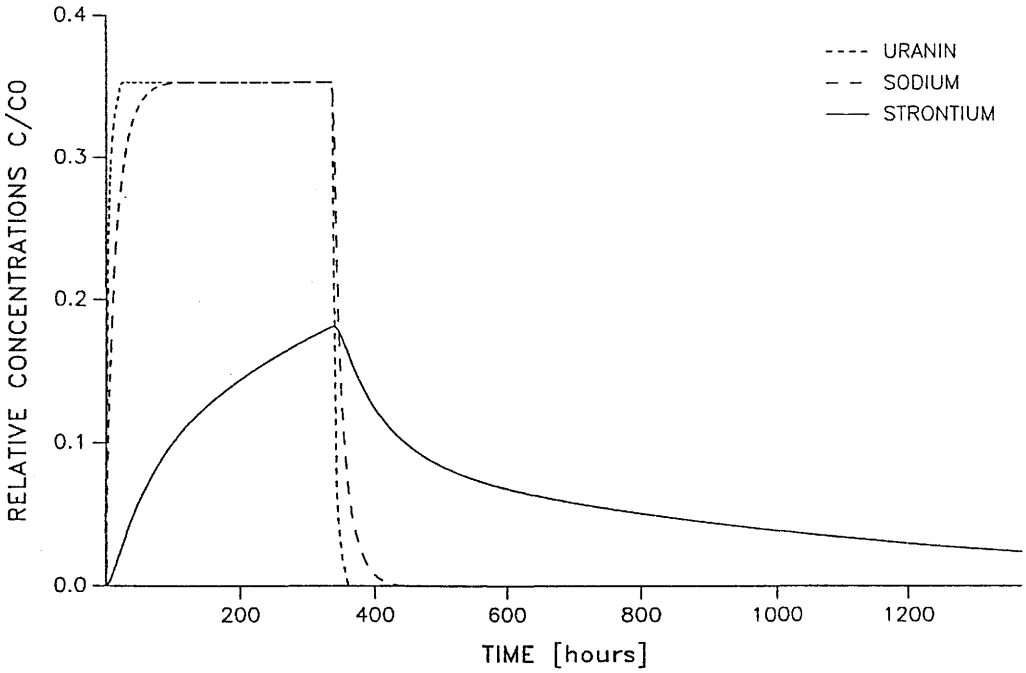

Figure 17: Tracer breakthrough curves in case of a step input test. The plateau at 0.35 corresponds to a dilution factor of $1/\beta$. Step duration is 336 hours.

From Fig. 17 the following is obvious:

Not for each K_d–value a plateau can be reached within an experimentally feasible time; this, of course, is crucial and should be kept in mind in designing a step input experiment. It probably is a good thing to perform a short pulse test first, extract an approximate K_d and make a prediction for an experimentally feasible step input migration test. The behaviour of the breakthrough curves for K_1 and K_2 does not hide any surprises; it is due to expectation.

6 Summary and Conclusions

In this report a very simple migration model is presented, in order to understand and predict migration experiments presently conducted at the Grimsel Test Site (GTS) of NAGRA in central Switzerland. The migration model has three building blocks:

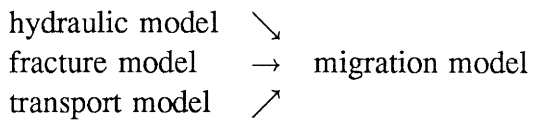

i) The hydraulic model is based on two experimental observations: 1) The migration zone is located in a planar fracture, and exhibits little interconnection with other waterbearing fissures; and 2) the hydraulic head difference between the boreholes 4 and 6 is very small showing a flat and homogeneous flow field in the region of interest.

   As all experimental arrangements have been chosen to be asymmetric dipoles, the hydraulic potential field is assumed to be the superposition of injection well and withdrawal well in a homogeneous medium. The resulting flow field is divided into a number of streamtubes, each characterized by appropriately defined streamfunctions. The flow rate within a streamtube as well as its length and transit time are unambiguously fixed. Solutes are transported advectively along each streamtube.

ii) The fracture with its layered infill is modelled as a plane parallel fracture where the infill porosity is visualized as a number of open plane parallel microfractures separated by the infill matrix. Solutes are transported advectively in each microfracture (in the same plane as the flow field) and diffused into the matrix of the infill material perpendicularly to the flow plane.

iii) The transport model, based on the model that led to the code RANCHMD, includes advective transport along each streamtube, matrix diffusion into the fracture infill and possibly sorption into the matrix (K_a=O was chosen because the surface adjacent to the open microchannels is given by the matrix). The breakthrough curve at the outlet is then the weighted superposition of breakthrough curves of each individual streamtube; the weight is given by the appropriate flow rate in the streamtube. The superposition of the breakthrough in the steamtubes is multiplied by a dilution factor which is determined by the ratio of the input to the output flow rate.

The model has been confronted with two experiments, Vorversuch 3 (uranine) and Vorversuch 29 (uranine and ^{24}Na). As a mathematically sound fit procedure has not been applied (cpu–time of up to

14 days would be needed for one experiment), fits by eye were conducted. The parameters extracted agree reasonably well with expectations and laboratory values [10]. Since it is not clear, whether the parameters extracted in this crude fashion correspond to the global minimum of a χ^2 function in parameter space (for the problem at hand the parameter space is 4–dimensional), a parameter variation study has been conducted for pulse tests. The results of that study are summarized as follows: For the type of hydraulic arrangements (such as matrix diffusion constant or matrix thickness, asymmetric dipole with $\beta = Q_w/Q_i \gtrsim 4$), non–sorbing tracers are not sensitive to matrix properties, at least in the range of variation because the matrix becomes saturated in all the within a couple of hours cases considered. There is a mild dependence of the time to reach saturation on the dispersion length a_L. For sorbing tracers the situation is some what more complicated: As long as the matrix is not saturated, the three parameters D_p (matrix diffusion constant), n (number of microfractures) and K_d (matrix sorption coefficient) are anticorrelated. Increasing the value of one parameter (with respect to a base case) and decreasing the value of another leads to a similar result as the base case. This is no longer true if the matrix becomes saturated within a timescale typical for the breakthrough curves: Parameters, which would lead to a reasonable fit in the unsaturated case, yield model results, which do not reproduce experimental curves any longer. Therefore, the judgement whether a fit-by-eye is reasonable strongly depends on the question whether one is able to decide, if matrix saturation occurred or not; step input experiments, where saturation is a condition to reach a plateau (its value given by the dilution factor) do not have that problem, and a fit-by-eye should yield parameters that are close to the χ^2 minimum.

Acknowledgements

The concept of the transport model described in this report is based on several fruitful discussions with J. Hadermann. Conclusions and suggestions based on the first model results could be clearly formulated after discussions with J. Hadermann and M. Bradbury. At this place I would like to thank them for their interest and encouragement.

References

[1] E. Hoehn, Th. Fierz, P. Thorne, "Hydrological Characterisation of the Migration Experiment Area at the Grimsel Test Site", PSI–Bericht Nr. 60, 1990, NTB 89-15.

[2] F. Herzog, "Hydrologic Modelling of the Migration Site in the Grimsel Rock Laboratory – The Steady State", PSI Bericht Nr. 35, 1989, NTB 89-16.

[3] e.g. J. Bear, "Hydraulics of Groundwater", Mc Graw Hill, New York NY, 1979, p. 167.

[4] S. Vomvoris, "Some results for unequal dipole tests", Nagra Internal Note, 1988.

[5] J. Hadermann, F. Roesel, "Radionuclide Chain Transport in Inhomogeneous Crystalline Rocks; Limited Matrix Diffusion and Effective Surface Sorption", EIR Bericht Nr. 551, 1985, NTB 85-40.

[6] W.H. Press, B.P. Flannery, S. A. Teukolsky, W.T. Vetterling, "Numerical Recipes", Cambridge University Press, Cambridge UK, 1989.
P.A. Smith, "Modelling of a Diffusion Sorption Experiment on Sandstone", PSI–Bericht Nr. 53, 1989.

[7] P. Steffen, H. Steiger, "Traceruntersuchungen Vorversuche 1 – 4, Rohdaten und Grafiken", Gemag, CH–6248 Alberswil, 1988.

[8] Th. Fierz, "Test Summary Vorversuch 29", Internal Report Solexperts, CH–8603 Schwerzenbach, 1989.

[9] J. Meyer, M. Mazurek, W.R. Alexander, in "Laboratory Investigations in Support of the Migration Experiments at the Grimsel Test Site", edited by M. H. Bradbury, PSI–Bericht Nr. 28, 1989, NAGRA NTB 88-23.

[10] J. Eikenberg, B. Baeyens, M.H. Bradbury, "The Grimsel Migration Experiment: A Hydrogeochemical Equilibrium Test", 1991, PSI–Bericht Nr. 100.